Generalized Analysis-oriented Model of FRP Confined Concrete Circular Columns

Javad Shayanfar [1], Joaquim A. O. Barros [2] and Mohammadali Rezazadeh [3]

[1] PhD Candidate, ISISE, Department of Civil Engineering, University of Minho, Azurém 4800-058 Guimarães, Portugal, arch3d.ir@gmail.com (corresponding author)

[2] Full Prof., ISISE, IBS, Department of Civil Engineering, University of Minho, Azurém 4800-058 Guimarães, Portugal, barros@civil.uminho.pt

[3] Lecturer, Civil Eng., Department of Mechanical and Construction Engineering, Northumbria University, Newcastle upon Tyne, NE1 8ST, United Kingdom, mohammadali.rezazadeh@northumbria.ac.uk

Abstract

This study is dedicated to the development of a generalized confinement model applicable to circular concrete columns confined by FRP full and partial confinement arrangements. To simulate the axial stress versus strain curve, a new strength model is proposed addressing the relation of axial stress and confinement pressure during axial loading, whose calibration was based on an extensive set of test results. By combining theoretical basis and experimental observations, the influence of non-homogenous distribution of concrete transversal expansibility with full/partial confinement during axial compressive loading is taken into the account in the establishment of confinement stiffness index. To estimate the ultimate condition of FRP fully/partially confined concrete, a new model with a design framework is also developed. It is demonstrated that global axial stress-strain curves and also dilation responses simulated by the proposed confinement model are in good agreement with those registered experimentally in available literature, and provides better predictions in terms of ultimate axial stress/strain than the formulations proposed by design standards.

Keywords: FRP confined columns; FRP confinement; Axial behavior; Dilation behavior; Confinement stiffness index

Notations

A_g	Total area of circular cross-section columns	n_f	FRP layer number
c_1	Non-dimensional empirical coefficient	R_1	Non-dimensional empirical coefficient
D	Diameter of circular column	R_2	Non-dimensional empirical coefficient
E_c	Concrete modulus elasticity	R_f	Non-dimensional parameter as s_f / D
E_f	FRP modulus elasticity	s_f	Distance between FRP strips
f_c	Axial stress corresponding to ε_c	t_f	FRP thickness
f_c^{Active}	Axial stress of AFC corresponding to ε_c	$k_{\varepsilon,min}$	Minimum value of k_ε^{FFC}
f_c^{Passive}	Axial stress of passively confined concrete at ε_c	L_d	Damage zone length of FRP confined concrete
f_{c0}	Peak compressive stress of unconfined concrete	L_{d0}	Damage zone length of unconfined concrete
f_{cc}^{Active}	Peak axial stress of AFC	w_f	FRP width
f_{cc}^{Passive}	Peak axial stress of passively confined concrete	ε_c	Axial strain corresponding to f_c
f_{cc}	Peak axial stress of FFC/FPC	ε_{c0}	Axial strain corresponding to f_{c0}
f_f	FRP confining stress	$\varepsilon_{c,m}$	Axial strain corresponding to $v_{s,max}$
f_f^{FFC}	FRP confining stress for FFC	ε_{cc}	Axial strain corresponding to f_{cc}
f_f^{FPC}	FRP confining stress for FPC	ε_{cu}	Ultimate axial strain
f_f^{*FFC}	Uniform FRP confining stress for FFC	$\varepsilon_{cu,c}$	Ultimate axial strain at concrete crushing
$f_{l,f}$	FRP confinement pressure	$\varepsilon_{cu,r}$	Ultimate axial strain at concrete crushing
$f_{l,f}^{FFC}$	FRP confinement pressure for FFC	ε_{fu}	Ultimate FRP tensile strain
$f_{l,f}^{*FFC}$	Uniform FRP confinement pressure for FFC	ε_h	FRP hoop strain
H	Column height	$\varepsilon_{h,max}$	Maximum FRP hoop strain
I_f	Confinement stiffness index	$\varepsilon_{h,rup}$	FRP hoop rupture strain
K_e	Confinement efficiency factor	$\varepsilon_l(z)$	Concrete lateral strain
k_{ff}	Reduction factor	$\varepsilon_{l,i}$	Concrete expansion at the mid-plane of FRP strips
k_{ff}^{FFC}	Reduction factor k_{ff} for FFC	$\varepsilon_{l,j}$	Lateral concrete expansion at the critical section
k_{ff}^{FPC}	Reduction factor k_{ff} for FPC	ε_V	Volumetric strain
$k_{v,f}$	Reduction factor	$\rho_{K,f}$	FRP confinement stiffness index
k_ε^{FFC}	Reduction factor for FFC	v_s	Secant Poisson's ratio
k_ε^{FPC}	Reduction factor for FPC	$v_{s,0}$	Initial Poisson's ratio of unconfined concrete
N	Total number of the fitted points	$v_{s,max}$	Maximum Poisson's ratio at the critical section
n	Concrete brittleness	$v_{t,eff}$	Effective tangential Poisson's ratio

1- Introduction

The reliability of fiber-reinforced-polymer (FRP) composites in various axial/shear/flexural strengthening scenarios has been demonstrated at laboratory level, as well as in real case applications in order to retrofit vulnerable as-built RC columns over seismic actions. For the case of axial strengthening, based on numerous experimentally, numerically, and theoretically conducted studies, it is now well-established that the application of FRP lateral confinement arrangements is efficiently capable of inducing improvements in terms of axial strength and deformability due to the curtailment of concrete lateral expansibility.

An experimental study conducted by Oliveira *et al.* [1] revealed that the capability of confinement strategy for improving the axial response of FRP fully confined concrete columns (FFC as illustrated in Fig. 1) is a function of the type of FRP material, concrete compressive strength, and confinement stiffness, which was also confirmed by Lim and Ozbakkaloglu [2-4]. Zeng *et al.* [5] have experimentally evaluated the efficiency of partial confinement arrangements using carbon fiber-reinforced polymer (CFRP) for increasing the load carrying capacity of concrete columns. The test results demonstrated that the axial and dilation responses of FRP partially confined concrete columns (FPC as illustrated in Fig. 1) strongly depend on the distance between consecutive strips (s_f) as a key parameter, besides the strip thickness and width, and the used FRP material properties. Barros and Ferreira [6] evidenced that by increasing s_f, the axial and dilation responses of FPC drove to be similar to those of unconfined concrete (UC), as verified by Zeng *et al.* [7]. For the case of FPC, Guo *et al.* [8, 9] and Janwaen *et al.* [10, 11] showed that concrete at the middle distance between two consecutive FRP strips, known as critical section, would be subjected to the maximum transversal deformation in comparison with the concrete expansion at the strip regions.

Numerous confinement models, known as analysis-oriented model (i.e. [3, 12-15]), have been proposed to simulate global axial stress-strain of FFC. Based on the implemented methodology for the establishment of axial stress-strain relationship, these models can be generally classified into three categories as demonstrated in Table 1. Category I (i.e. Lim and Ozbakkaloglu [15]) includes models for actively confined concrete columns (AFC), where the concrete is subjected to an active confinement pressure (f_l^{Active}), with a constant value during entire axial loading, as illustrated in Fig. 1b. In this case, axial stress (f_c^{Active}) at a certain axial strain (ε_c) can be determined by adopting an axial stress-strain relation (i.e. Popovics [16] suggested for AFC), expressed as a main function of peak axial stress (f_{cc}^{Active}), leading to $f_c^{Active} = g_1\left(f_{cc}^{Active}\right)$, henceforth designated by stress-strain base relation. In this case, as the most widely adopted framework to date, f_{cc}^{Active} is generally determined as $f_{cc}^{Active} = g_2\left(f_l^{Active}\right)$ depending on f_l^{Active} as demonstrated in Table 1. Several studies have been carried out to suggest the calibration factors of m_{a1} and m_{a2} for the g_2 function (Table 1) through using a regression analysis-based method on a set of test database of AFC, which presents the effectiveness of confinement strategy in axial strength enhancements. In Category II (i.e. [12-14]), conventionally, by adopting a stress-strain base relation, for the case of FFC under a FRP confinement pressure ($f_{l,f}^{*\,Passive}$) assumed to be homogenously imposed to the entire column height with a variable value during axial loading (Figs. 1b and 1c) , its axial stress ($f_c^{Passive}$) at a certain ε_c is considered to be identical to f_c^{Active} through taking into account $f_l^{Active} = f_{l,f}^{*\,Passive}$ ($f_c^{Passive} = g_1\left(f_{cc}^{Passive}\right)$). However, studies conducted by Lim and Ozbakkaloglu [3], Lin *et al.* [17] and Yang and Feng [18] demonstrated that this approach, whose development is based on the calibration of m_{a1} and m_{a2} for AFC (Table 1), would lead to overestimations in predicting global

axial stress-strain relation of FFC (Δf_c), even though $f_{l,f}{}^{Active} = f_{l,f}{}^{Passive}$ at a certain ε_c, as highlighted in Fig. 1b-d. It can be attributed to the considerable difference in the confinement pressure path imposed to concrete in AFC and FFC with constant and variable trends, respectively, as presented in Fig. 1b. Confinement pressure path in the present context represents the relation between confinement pressure and axial stress/strain during the entire axial compressive loading. Category III includes analysis-oriented models formulating the noticeable influence of confinement pressure path on axial response of FFC. In this category, Lim and Ozbakkaloglu [3] introduced the concept of a reduced stress-strain base relation for the case of FFC to reflect this effect in the calculation of $f_{cc}{}^{Passive}$ through applying a reduction Δf_l in the actual FRP confinement pressure obtained from dilation model. In this model, as presented in Fig. 1b, Δf_l represents the gradient of confinement pressure that was suggested empirically as a function of confinement stiffness (known as the ratio of FRP confinement pressure over concrete lateral strain), concrete compressive strength and the corresponding concrete lateral strain. Yang and Feng [18] proposed a refined version of Jiang and Teng [12]'s model (Category II) to account for the difference in confinement pressure paths of FFC and AFC in terms of the peak axial stress of the stress-strain base relation (Δf_{cc}). In this approach, the calibration factors of m_{p1} and m_{p2} (Table 1) were derived from a set of test results of FFC specimens. It was also demonstrated that this effect plays a key role in the establishment of global axial stress-strain response of FCC. Based on Zhao *et al.* [19]'s model originally suggested for concrete-filled steel tube columns, Lin *et al.* [17] investigated the influence of confinement pressure path on ultimate axial stress of FFC, which was demonstrated to be a function of the level of confinement pressure at FRP rupture and concrete compressive strength. By considering this effect in the establishment of ultimate axial stress of FFC, the model demonstrated a better performance in predicting the experimental counterparts.

Nonetheless, to the best of the authors' knowledge, the substantial influence of confinement pressure path on axial stress-strain response of FPC has not been investigated comprehensively in the existing models. Accordingly, the development of a confinement model addressing confinement pressure path to predict the global axial-stress-strain of FPC with a unified approach with FFC is still lacking.

On the other hand, in existing analysis-oriented models, in general, for the sake of the simplicity, by assuming a uniform distribution of concrete expansion for FFC, confinement pressure ($f_{l,f}^{*\ Passive}$) is subsequently considered to be homogenous along the column height. However, this assumption is only acceptable prior to the loading stage corresponding to the peak axial stress of unconfined concrete. Beyond this stage, the rate of concrete lateral expansion tends to significantly increase due to the development of longitudinal concrete cracking, leading to a non-uniform distribution of concrete transversal dilatancy, particularly in the case of FRP lightly confined concrete [20-22]. Wu and Wei [20] performed axial compressive tests on FFC, FPC and unconfined concrete (UC) columns to examine the distribution of concrete lateral strain along the column height. It was highlighted that during axial loading, concrete would experience a non-uniform distribution of expansion depending on confinement configuration. To evaluate the influence of confinement on concrete axial/lateral strain distribution of FFC along the column height, Fallahpour *et al.* [22] conducted an experimental investigation through Digital Image Correlation (DIC) technique for the measurement of full- field strain evolution. The test results demonstrated that FFC only with high confinement stiffness revealed relatively homogenous axial and dilation responses, while in the case of lower confinement stiffness, less uniform behavior along with local strain gradients was exhibited. Therefore, since the generation of FRP confining hoop strain/stress is in a direct relation with concrete dilation behavior, the generated confining stress would be imposed non-

116 homogenously on the concrete as a main function of confinement stiffness. As a result, the
117 assumption of uniform confinement pressure ($f_{l,f}^{*\ Passive}$) can be considered to be acceptable only
118 for highly-confined concrete. For the case of low confinement stiffness with non-homogenous
119 confining stress distribution, this assumption does not seem to adequately comply the described
120 experimental observations. For the case of FPC, Zeng *et al.* [7] experimentally evidenced the
121 distribution of concrete expansion would be predominantly non-homogenous, particularly in case
122 of large s_f (distance between strips of FRP, Fig. 1a), as also confirmed by Guo *et al.* [8, 9].
123 Shayanfar *et al.* [23] presented a refined version of the concept of confinement efficiency factor,
124 originally suggested by Mander *et al.* [24] for concrete confined partially with steel stirrups, by
125 formulating the non-homogenous distribution of concrete dilatancy of FPC, besides the influence
126 of vertical arching action. However, in this model, the pattern of concrete expansion of FFC was
127 assumed as uniform, for the sake of simplicity. Therefore, to the best of the authors' knowledge,
128 the influence of non-homogenous distribution of concrete expansion along the column height of
129 FFC/FPC on the determination of confinement pressure and subsequently, axial and dilation
130 responses has not been addressed comprehensively in the existing analysis/design-oriented
131 models.

132 The present study is dedicated to the development of a generalized confinement model, applicable
133 to full and partial confinement arrangements applied on circular cross section concrete columns,
134 by using a unified approach in the prediction of their axial and dilation responses. For formulating
135 the influence of concrete expansion distribution in the calculation of confinement pressure,
136 Shayanfar *et al.* [23]'s model is extended to be applicable to FFC as a function of confinement
137 stiffness, along with some refinements for the case of FPC. A new analysis-oriented model as
138 confinement-path dependent in compliance with Category III is proposed for the establishment of

the axial stress-strain curve of FFC and FPC, by introducing new calibration factors of m_{p1} and m_{p2} depending on confinement stiffness. A new expression is subsequently developed to estimate ultimate axial strain of FFC/FPC by combining theoretical knowledge and experimental observations. Finally, the reliability of the developed model is vastly examined by simulating the global axial stress-strain curves registered experimentally in available literature. The comparative assessment of the predicted performance in term of ultimate axial stress/strain obtained from the developed model versus by *fib* [25], CNR DT 200/2004 [26] and ACI 440.2R-17 [27] approaches (briefly presented in Appendix A) is also demonstrated.

2- Proposed confinement model for FFC

This section provides the determination of the confinement characteristics of FFC under axial compressive loading. The effectiveness of FRP confining system to limit concrete dilatancy during axial loading is dependent on the level of confinement pressure. For the case of full confinement with a uniform concrete expansibility along the column height (assuming identical hoop and radial strain $\varepsilon_h = \varepsilon_{l,j}$), the FRP confining stress, $f_f^{*\,FFC}$, and the FRP confinement pressure, $f_{l,f}^{*\,FFC}$, can be derived using force equilibrium conditions (Fig. 1a):

$$f_{l,f}^{*\,FFC} = 2\frac{n_f t_f}{D} f_f^{*\,FFC} = 2\frac{n_f t_f}{D} E_f \varepsilon_{l,j} \tag{1}$$

where n_f is the number of FRP layers, t_f is the FRP thickness, D is the diameter of the column, E_f is the FRP modulus elasticity, and $\varepsilon_{l,j}$ is the maximum concrete lateral expansibility along with the assumption of perfect bond between FRP and concrete substrate. Nevertheless, the studies conducted by Wu and Wei [20] and Wei and Wu [21] demonstrated that the distribution of the concrete lateral expansion in the case of FFC system during axial compressive loading would vary

along the column height as a function of confinement stiffness. As shown in Fig. 2, the maximum ($\varepsilon_{l,j}$) and minimum ($\varepsilon_{l,i}$) concrete lateral expansibility can be assumed to occur at the Point *j* and Point *i*, respectively, with the distance of L_d defining the damage zone length, which will be addressed in detail in Section 3. Consequently, at a certain level of $\varepsilon_{l,j}$, the maximum and minimum FRP confining stresses are $f_{f,j}^{FFC} = E_f \varepsilon_{l,j}$ and $f_{f,i}^{FFC} = E_f \varepsilon_{l,i}$, respectively. In this study, the reduction factor k_{ff} is introduced to determine an average FRP confining stress (f_f^{FFC}) uniformly applied on the columns in order to account for the non-uniform concrete expansibility:

$$f_f^{FFC} = k_{ff}^{FFC} f_{f,j}^{FFC} = k_{ff}^{FFC} E_f \varepsilon_{l,j} \tag{2}$$

Based on Eq. (1), FRP confinement pressure ($f_{l,f}^{FFC}$) resulting from f_f^{FFC} can be expressed as:

$$f_{l,f}^{FFC} = 2\frac{n_f t_f}{D} f_f^{FFC} = 2\frac{n_f t_f}{D} k_{ff}^{FFC} E_f \varepsilon_{l,j} \tag{3}$$

For the sake of simplicity, the reduction factor k_{ff}, can be determined by taking an average of the $\varepsilon_l(z)/\varepsilon_{l,j}$ ratio along the damage zone (Fig. 3):

$$k_{ff}^{FFC} = 2\frac{\int_0^{L_d/2} \frac{\varepsilon_l(z)}{\varepsilon_{l,j}} dz}{L_d} = 2\frac{\int_0^{L_d/2} k_\varepsilon(z) dz}{L_d} \tag{4}$$

where $\varepsilon_l(z)$ defines the concrete lateral strain within the damage zone (L_d) along the *z* axis as illustrated in Fig. 3. Considering a second order parabola function distribution for $k_\varepsilon(z)$ along with $k_\varepsilon = k_\varepsilon^{FFC}$ and $dk_\varepsilon(z)/dz = 0$ at the point *i* ($z = L_d/2$), leads to (Fig. 3):

$$k_{ff}^{FFC} = \frac{2\int_0^{L_d/2}\left(a_1 z^2 + a_2 z + a_3\right)dz}{L_d} = \frac{2\int_0^{L_d/2}\left[1-4\left(1-k_\varepsilon^{FFC}\right)\left(\frac{z}{L_d}-\left(\frac{z}{L_d}\right)^2\right)\right]dz}{L_d} = \frac{1}{3}+\frac{2}{3}k_\varepsilon^{FFC} \quad (5)$$

where k_ε^{FFC} is the ratio between $\varepsilon_{l,i}$ and $\varepsilon_{l,j}$. For highly-confined concrete by FRP confinement pressure, concrete transversal expansibility tends to be uniform, leading to $k_\varepsilon^{FFC}=1$ and according to Eq. (5), $k_{ff}^{FFC}=1$. In this case, the volumetric strain would be positive during axial compressive loading ($\varepsilon_V \geq 0$), as shown in Fig. 4, representing a specimen's volume decrease. On the other hand, lightly-confined concrete experiences a noticeable variation in expansion, depending on the confinement stiffness. In this study, based on Teng *et al.* [28] achievements, for FFC with uniform concrete expansibility, confinement stiffness index I_f can be determined as:

$$I_f = \frac{f_{l,f}^{FFC}/\left(k_{ff}^{FFC}\varepsilon_{l,j}\right)}{f_{c0}/\varepsilon_{c0}} = 2\frac{n_f t_f E_f \varepsilon_{c0}}{D f_{c0}} \quad (6)$$

in which

$$\varepsilon_{c0} = 0.0015 + \frac{f_{c0}}{70000} \qquad (f_{c0} \text{ in MPa}) \quad (7)$$

where ε_{c0} is the axial strain corresponding to f_{c0}, as suggested by Karthik and Mander [29]. Fig. 4 shows the relation between the normalized axial stress (f_c/f_{c0}) and volumetric strain ($\varepsilon_V = \varepsilon_c - 2\varepsilon_{l,j}$) for the test specimens conducted by Wang and Wu [30], Eid *et al.* [31], Lim and Ozbakkaloglu [4] and Zeng *et al.* [5] with different I_f. As can be seen, the confinement configurations corresponding to the confinement stiffness index less than 0.045 are not capable of controlling concrete dilation, with concrete dilation as high as smaller is I_f. Teng *et al.* [28]

recommended that for lightly confined concrete ($I_f \le 0.01$), the effectiveness of confinement pressure on axial and dilation response can be neglected. At I_f of about 0.045, the volumetric strain evolution virtually becomes reversed due to FRP jacket capability to restrain the concrete expansion. For $I_f \ge 0.045$, since the FRP confinement pressure is significantly activated, the confined concrete drives to behave in a compaction way. Accordingly, for high value of I_f with $\varepsilon_V \ge 0$, the distribution of concrete expansion of FFC is expected to be approximately uniform with $k_\varepsilon^{FFC} = \varepsilon_{l,i} / \varepsilon_{l,j} \simeq 1$. To evaluate the influence of confinement on concrete axial/lateral strain distribution of FFC along the column height, Fallahpour *et al.* [22] experimentally evidenced that FFC only with high confinement stiffness ($I_f = 0.061$) revealed relatively homogenous axial and dilation responses, while in the case of lower confinement stiffness, less uniform behavior along with local strain gradients (leading to a low value of k_ε^{FFC}) was exhibited.

Based on the aforementioned discussion, using the dilation model developed by Shayanfar *et al.* [23] (Eq. (8)), when $\varepsilon_V = 0$, the value of confinement stiffness index (I_f^*) corresponding to the maximum secant Poisson's ratio ($v_{s,\max}$) equal to 0.5 can be determined by Eq. (9).

$$v_{s,\max} = \frac{0.155}{\left(1.23 - 0.003 f_{c0}\right)\sqrt{I_f}} \tag{8}$$

$$I_f^* = \left(\frac{0.155}{\left(1.23 - 0.003 f_{c0}\right) \times 0.5} \right)^2 \simeq 0.06 + 0.0005 f_{c0} \qquad (f_{c0} \text{ in MPa}) \tag{9}$$

Accordingly, based on the experimental observations conducted by Fallahpour *et al.* [22] for $I_f < I_f^*$, a non-uniform distribution of concrete expansion with maximum and minimum lateral

strains at Point *j* and Point *i*, respectively, can be assumed, so that $k_{\varepsilon}^{FFC} < 1$. Based on the above discussion, to develop the relation between k_{ε}^{FFC} and I_f, the following conditions should be satisfied:

i. k_{ε}^{FFC} enhances with increasing I_f.

ii. k_{ε}^{FFC} approaches the value of $k_{\varepsilon,\min}$ when confinement pressure is equal to zero (unconfined concrete).

iii. k_{ε}^{FFC} approaches 1 when $I_f \geq I_f^*$ as evidenced by Fallahpour *et al.* [22]

Shayanfar *et al.* [23, 32] recommended $k_{\varepsilon,\min} = 0.08$ based on the experimental dilation results of a series of unconfined concrete specimens. Considering the aforementioned conditions, a new expression was derived to determine k_{ε}^{FFC} from I_f and I_f^* (Fig. 5):

$$k_{\varepsilon}^{FFC} = 0.08 + 0.92\left[2\frac{I_f}{I_f^*} - \left(\frac{I_f}{I_f^*}\right)^2\right] \leq 1 \qquad \text{for } I_f \leq I_f^* \tag{10}$$

$$k_{\varepsilon}^{FFC} = 1 \qquad \text{for } I_f \geq I_f^* \tag{10}$$

Ultimately, by determining k_{ε}^{FFC} depending on I_f, k_{ff}^{FFC} can be obtained using Eq. (5) as an input parameter in Eq. (3) for the calculation of $f_{l,f}^{FFC}$.

3- Proposed confinement model for FPC

This section is dedicated to address the determination of the confinement characteristics of partially confined concrete (FPC) columns under axial compressive loading. In Fig. 6, the non-

uniform distributions of concrete lateral expansion and FRP partial confining stress in FPC are presented. As can be seen, the maximum expansion $\varepsilon_{l,j}$ would occur at the critical section corresponding to Point *j*, which is not directly subjected to confinement pressure. However, point *i* corresponding to middle section of FRP strip experiences the minimum concrete dilatancy, $\varepsilon_{l,i}$, leading to FRP confining stress $f_{f,i}$. In this study, according to Eqs. (1) to (3), considering the influence of vertical arching action based on Shayanfar *et al.* [32] presented in Eq. (14), FRP confinement pressure (${f_{l,f}}^{FPC}$) generated by ${f_f}^{FPC}$ can be expressed as:

$$ {f_{l,f}}^{FPC} = 2\frac{n_f t_f w_f}{\left(s_f + w_f\right)D} k_{v,f} {f_f}^{FPC} = 2\frac{n_f t_f}{D} k_\rho k_{v,f} {f_f}^{FPC} \tag{11} $$

in which

$$ {f_f}^{FPC} = {k_{ff}}^{FPC} {f_{f,j}}^{FPC} = {k_{ff}}^{FPC} E_f \varepsilon_{l,j} \tag{12} $$

$$ k_\rho = \frac{w_f}{s_f + w_f} \tag{13} $$

$$ k_{v,f} = \frac{w_f + s_f\left(1 - R_f + 0.43{R_f}^2 - 0.07{R_f}^3\right)}{w_f + s_f} \le 1 \qquad ([32]) \tag{14} $$

$$ R_f = \frac{s_f}{D} \tag{15} $$

where w_f is the strip width. R_f is a non-dimensional parameter. It should be noted that, due to vertical arching action mechanism between two consecutive strips, confinement pressure effectiveness on this zone can be very distinct from the one corresponding to full confinement. Based on the concept of the confinement efficiency factor ([24]), by applying the reduction factor

229 $k_{v,f}$, the entire concrete column can be assumed to be as effectively confined concrete, similar to
230 FFC confinement mechanism.

231 According to the developed relation for FFC ($s_f = 0$), by increasing s_f in FPC system, the
232 confinement system capability to curtail concrete transversal expansibility decreases. Accordingly,
233 for a relatively large value of s_f, the effectiveness of this partial confining system becomes
234 minimal and approaches to $k_{\varepsilon,\min} = 0.08$, while k_{ff}^{FPC} can be assumed as k_{ff}^{FPC} when $s_f = 0$. In
235 this study, for $s_f \geq L_d$, representing the condition that the damage zone occurs between FRP strips,
236 the effect of confinement was conservatively ignored and its dilation behavior would be similar to
237 that of unconfined concrete (Wei and Wu [21]). Consequently, for this case, L_d can be estimated
238 to be equal to the length of damage zone of unconfined concrete columns (L_{d0}). By using the
239 concept of localized compressive fracture length proposed by Lertsrisakulrat *et al.* [33], Wu and
240 Wei [20] recommended an empirical equation to calculate L_{d0} as a function of column diameter
241 and concrete compressive strength as follows (with a slight rearrangement):

$$0.57 \leq \frac{L_{d0}}{D_{Ler}\psi_f} = 1.71 - 3.53\times10^{-5} D_{Ler}^2 \leq 1.36 \tag{16}$$

242 in which

$$D_{Ler} = \sqrt{A_g} \simeq 0.886D \quad (D \text{ in MPa}) \tag{17}$$

$$\psi_f = \frac{6.3}{\sqrt{f_{c0}}} \leq 1 \quad (f_{c0} \text{ in MPa}) \tag{18}$$

where D_{Ler} is the equivalent diameter that is calculated as the square root of the total cross-sectional area [33].

To develop the relation between k_{ff}^{FPC} and s_f, the following conditions should be satisfied:

i. k_{ff}^{FPC} decreases with the increase of s_f.

ii. k_{ff}^{FPC} is equal to k_{ε}^{FPC} when $s_f \simeq L_{d0}$

iii. k_{ff}^{FPC} follows a hoop strain distribution similar to FFC when $s_f \simeq 0$

iv. k_{ff}^{FPC} approaches the value of $k_{\varepsilon,\min}$ when $s_f \simeq L_{d0}$ (unconfined concrete).

v. k_{ff}^{FPC} approaches k_{ff}^{FFC} when $s_f \simeq 0$.

Therefore, the relation between k_{ff}^{FPC} and s_f / L_{d0} was formulated to decrease linearly from $k_{ff}^{FPC} = k_{ff,ave}^{FPC}$ at $s_f = 0$ (full confinement) to $k_{ff}^{FPC} = 0.08$ at $s_f = L_{d0}$:

$$k_{ff}^{FPC} = k_{ff,ave}^{FPC} - \left(k_{ff,ave}^{FPC} - k_{\varepsilon}^{FPC}\right)\frac{s_f}{L_{d0}} \geq 0.08 \tag{19}$$

in which

$$k_{ff,ave}^{FPC} = \frac{1}{3} + \frac{2}{3}k_{\varepsilon}^{FPC} \tag{20}$$

where $k_{ff,ave}^{FPC}$ represents the ratio of average hoop strain and maximum hoop strain within the damage zone, based Eq. (5) with a uniform approach with FFP, when the distribution of concrete lateral strain would be identical to full confinement in the case of $s_f = 0$. Introducing Eq. (20) into Eq. (19) gives

$$k_{ff}^{FPC} = \frac{1}{3}\left(1+2k_{\varepsilon}^{FPC}\right) - \frac{s_f}{3L_{d0}}\left(1-k_{\varepsilon}^{FPC}\right) \geq 0.08 \quad (21)$$

For the determination of k_{ε}^{FPC}, based on Eq. (19), it was assumed that it linearly decreases from $k_{\varepsilon}^{FPC} = k_{\varepsilon}^{FFC}$ (at s_f / L_{d0} =0, full confinement) to $k_{\varepsilon}^{FPC} = 0.08$ (at $s_f = L_{d0}$) (Fig. 7):

$$k_{\varepsilon}^{FPC} = k_{\varepsilon}^{FFC} - \left(k_{\varepsilon}^{FFC} - 0.08\right)\frac{s_f}{L_{d0}} \geq 0.08 \quad (22)$$

Accordingly, by replacing k_{ε}^{FFC} obtained from Eq. (22) in Eq. (21), k_{ff}^{FPC} can be determined, as an input parameter in Eq. (12). The k_{ff}^{FPC} versus s_f / L_{d0} relationship for FPC is demonstrated in Fig 7. It estimates k_{ff}^{FPC} lower than Shayanfar *et al.* [23] model due to the consideration of a non-uniform distribution for concrete lateral expansion in case of FFC.

It is now well-established that the FRP confinement-induced improvements in FFC and FPC substantially depend on the confinement stiffness imposed on the confined concrete. For reflecting the influence of this parameter, the recommendation of Shayanfar *et al.* [23] was taken, by proposing a new confinement stiffness index applicable to both full and partial systems, taking into account the concrete transversal expansibility (by considering Eqs. (6), (11) and (12)):

$$\rho_{K,f} = \frac{f_{l,f}^{FPC} / \varepsilon_{l,j}}{f_{c0} / \varepsilon_{c0}} = k_{\rho} k_{v,f} k_{ff}^{FPC} I_f = K_e I_f \quad (23)$$

in which

$$K_e = k_{\rho} k_{v,f} k_{ff}^{FPC} \quad (24)$$

where K_e is defined as the confinement efficiency factor. For FFC, Eq. (23) leads to $\rho_{K,f} = k_{ff}^{FFC} I_f$ that can be calculated using Eqs. (5) and (6), respectively.

4- Dilation model

This section is dedicated to address the determination of the dilation characteristics for FFC and FPC. According to the confinement mechanism, at a certain axial stress, f_c, the corresponding ε_c leads to lateral strain $\varepsilon_{l,j}$ (radial strain) in compliance with concrete secant Poisson's ratio v_s, resulting in confining stress to restrain concrete tendency to dilate. By rearranging Eq. (23), FRP confinement pressure can become explicitly dependent on v_s:

$$\frac{f_{l,f}^{FPC}}{f_{c0}} = \rho_{K,f} \frac{\varepsilon_{l,j}}{\varepsilon_{c0}} = \rho_{K,f} \frac{v_s \varepsilon_c}{\varepsilon_{c0}} \tag{25}$$

Accordingly, the determination of v_s corresponding to ε_c is essential for calculating the confinement pressure. Based on a large database of the experimental dilation responses of FFC and FPC, Shayanfar *et al.* [23] proposed a strategy to calculate the relation between $v_s/v_{s,\max}$ and ε_c, as illustrated in Fig. 8. Here, $v_s/v_{s,\max}$ is the secant Poisson's ratio normalized by its maximum value at the critical section during axial loading corresponding to the axial strain of $\varepsilon_{c,m}$, which was empirically suggested as:

$$\varepsilon_{c,m} = 0.0085 - 0.05\rho_{K,f} \tag{26}$$

As shown in Fig. 8, the dilatancy of confined concrete is equal to that of unconfined concrete up to $\varepsilon_c = \varepsilon_{c0}$ (point A) with $v_s = v_{s,0}$, which can be calculated by (Candappa *et al.* [34]):

$$v_{s,0} = 8\times10^{-6} {f_{c0}}^2 + 2\times10^{-4} f_{c0} + 0.138 \quad (f_{c0} \text{ in MPa}) \tag{27}$$

Since the development of concrete cracking induces an increase in v_s, the trend evolves from $v_{s,0}$ to $c_1 \times v_{s,max}$ (point B), corresponding to $\varepsilon_c = 2\varepsilon_{c0}$ ([25]), and further increases up to $v_{s,\max}$ at $\varepsilon_c = \varepsilon_{c,m}$ (point C), followed by a decrease until ultimate conditions. To formulate the relation between v_s and ε_c, the determination of $v_{s,\max}$ as an input parameter is necessary, which was derived empirically through regression analysis method. The test database (Table 2), used for deriving/calibrating the model parameters in the present study, consists of the test specimens of FFC and FPC with a wide range of material properties. It comprises $70 \le D \le 300$ (mm), $15.8 \le f_{c0} \le 171.0$ (MPa), $13.6 \le E_f \le 276.0$ (MPa), $0.013 \le \varepsilon_{fu} \le 0.035$, $0.001 \le \rho_{K,f} \le 0.262$ and different FRP types as carbon, glass, basalt and aramid FRP (CFRP, GFRP, BFRP, AFRP).

Fig. 9a demonstrates the variation of $v_{s,\max}$ with $\rho_{K,f}$ based on the test database by Shayanfar *et al.* [23]. As expected, the $v_{s,\max}$ decreases with the increase of the confinement stiffness, as $v_{s,\max} = 0.15/\sqrt{\rho_{K,f}}$ using a preliminary regression analysis (Fig. 9a). The decrease is quite abrupt up to $\rho_{K,f} \cong 0.015$, and smooth above this value. In the present study, based on the best fit with experimental results, a new formulation to calculate $v_{s,\max}$ as a main function of $\rho_{K,f}$ (along with L_{d0}/D) was developed, resulting in:

$$v_{s,\max} = \frac{0.15}{\left(0.585 + 0.585\frac{L_{d0}}{D}\right)\sqrt{\rho_{K,f}}} = \frac{0.256}{\left(1 + \frac{L_{d0}}{D}\right)\sqrt{\rho_{K,f}}} \tag{28}$$

The acceptable predictive performance of Eq. (28) in the simulation of the experimental counterparts can be confirmed in Fig. 9b.

5- Model to determine the axial stress-strain response

This section addresses the establishment of the axial stress-strain relation of circular cross section concrete columns with FFC and FPC arrangements. A new model in compliance with Category III is proposed by introducing new calibration factors of m_{p1} and m_{p2} as presented in Table 1. In this category, at a certain level of axial strain (ε_c), the corresponding axial stress (f_c) can be determined by adopting a stress-strain base relation, whose characteristics are expressed as a function of the peak stress (f_{cc}) and the corresponding axial strain (ε_{cc}).

To formulate f_c versus ε_c relation as a stress-strain base relation, the expression suggested by Popovics [16], originally for AFC, was adopted:

$$f_c = f_{cc}\frac{(\varepsilon_c/\varepsilon_{cc})n}{n-1+(\varepsilon_c/\varepsilon_{cc})^n} \tag{29}$$

in which

$$\frac{\varepsilon_{cc}}{\varepsilon_{c0}} = 1+5\left(\frac{f_{cc}}{f_{c0}}-1\right) \qquad ([25]) \tag{30}$$

$$n = \frac{E_c}{E_c - f_{cc}/\varepsilon_{cc}} \tag{31}$$

$$E_c = 4400\sqrt{f_{c0}} \qquad (f_{c0} \text{ in MPa}) \tag{32}$$

where n defines the concrete brittleness introduced by Carreira and Chu [47]; E_c is the modulus elasticity of concrete proposed by Lim and Ozbakkaloglu [15].

In the present study, according to Yang and Feng [18], a new strength model in compliance with Category III (Table 1) is developed to determine the relation between f_{cc} and $f_{l,f}^{FPC}$ (which is

determined from Eq. (25)), derived from global axial stress-strain of FFC/FPC test specimens with passive confinement path. It can be expressed as

$$\frac{f_{cc}}{f_{c0}} = 1 + m_{p1}\left(\frac{f_{l,f}^{*\ Passive}}{f_{c0}}\right)^{m_{p2}} = 1 + \frac{R_1}{R_2}\left(\frac{f_{l,f}^{\ FPC}}{f_{c0}}\right)^{R_2} = 1 + \frac{R_1}{R_2}\left(\rho_{K,f}\frac{v_s\varepsilon_c}{\varepsilon_{c0}}\right)^{R_2} \tag{33}$$

where R_1 and R_2 are the terms introduced to calibrate this equation. For this purpose, the extracted experimental R_1 and R_2 were determined using back analysis method performed on the global axial stress-strain of FFC/FPC test specimens. It is because that contrary to the case of AFC in which $f_{cc}^{\ Active}$ as a function of $f_l^{\ Active}$ is constant during entire axial loading, f_{cc} significantly varies with $f_{l,f}^{\ FPC}$ in the case of passive confinement. Accordingly, calibrating Eq. (33) just based on the failure stage of the test specimens does not sufficiently reflect the relation of f_{cc} and $f_{l,f}^{\ FPC}$. Therefore, in the present study, considering the variable relation of f_{cc} and $f_{l,f}^{\ FPC}$ depending on the level of axial strain, based on the best fitting with the experimental f_c vs ε_c curves collected in the test database, these parameters as a main function of the developed confinement stiffness index ($\rho_{K,f}$) were determined as,:

$$R_1 = \frac{23.9\rho_{K,f}^{\ 0.67}}{\lambda_{fc}\lambda_{Rf}\lambda_D} \le 4.25 \tag{34}$$

$$R_2 = 1.85\rho_{K,f}^{\ 0.26} \ge 0.3 \tag{35}$$

in which

$$\lambda_{fc} = 0.75 + 0.008 f_{c0} \qquad (f_{c0} \text{ in MPa}) \tag{36}$$

$$\lambda_{Rf} = 1 + 0.5R_f \quad (37)$$

$$\lambda_D = 0.82 + 0.0012D \geq 1 \quad (D \text{ in MPa}) \quad (38)$$

where λ_{fc} , λ_{Rf} and λ_D are the calibration terms introduced to reflect the influence of f_{c0}, R_f and D in Eq. (34). To highlight the correlations of Eqs. (34 and 35), the developed R_1 and R_2 were compared to the extracted experimental results in Fig. 10. The statistical indicates show that the proposed equations for these parameters estimate the experimental counterparts of FFC/FPC with acceptable accuracy. It should be noted that since the proposed confinement model was developed with a uniform approach for FFC and FPC, Eq. (33) can be considered valid for both cases. The incremental calculation procedure based on the developed model to determine the axial response of FFC/FPC with $\rho_{K,f}$ is as follows:

1- Assume a value of ε_c
2- Calculate the secant Poisson's ratio v_s as a function of $\rho_{K,f}$ (from Fig. 8 considering Eqs. (26-28))
3- Calculate the peak axial stress f_{cc} using Eq. (33)
4- Calculate the peak axial stress ε_{cc} using Eq. (30)
5- Calculate the axial stress f_c using Eq. (29)
6- Continue the steps 1-5 up to ultimate condition.

6- Ultimate condition

In this section, a new methodology will be introduced to determine ultimate axial strain of FFC and FPC under axial compressive loading. According to failure mechanism of FFC (Fig. 11a),

348 when the maximum concrete hoop strain along the column height reaches FRP ultimate hoop strain
349 ($\varepsilon_{h,rup}$), the confinement provided by the FRP is lost, followed by an abrupt column's load decay.
350 However, in the case of FPC with a large s_f, damage tends to initiate by concrete spalling, and
351 the specimen finally fails as concrete crushing along with inclined concrete cracking between FRP
352 strips, as illustrated in Fig. 11e. In this case, as concrete lateral expansion at the critical section
353 increases, FRP hoop strain at the mid-plane of the strips, generating lateral confinement, does not
354 enhance considerably due to lower concrete expansion. Accordingly, the failure mechanism can
355 be regarded as that of unconfined concrete. However, by decreasing s_f, since expansion at the
356 mid-plane of the strips would increase, the confined column would fail due to rupture of FRP
357 jacket (Fig. 11b-d). According to the failure mechanism of partially confined columns, concrete
358 lateral expansion increases until hoop rupture of FRP jacket along with concrete crushing
359 simultaneously. The concrete crushing seems to be more probable in the case of the specimens
360 with larger R_f due to a substantial increase in ineffective confinement area.

361 In this study, for the calculation of the ultimate axial strain (ε_{cu}), a unified model with a design
362 framework was developed applicable to both cases of FFC and FPC based on a combination of
363 theoretical basics and regression analysis. For the case of FFC, when maximum hoop strain ($\varepsilon_{h,\max}$
364) in FRP jacket reaches FRP hoop rupture strain, $\varepsilon_{h,rup}$, the corresponding $v_{s,u}$ depending on
365 $\varepsilon_{cu} = \varepsilon_{cu,r}$ can be determined as:

$$v_{s,u} = \frac{\varepsilon_{h,\max}}{\varepsilon_{cu,r}} = \frac{\varepsilon_{h,rup}}{\varepsilon_{cu,r}} \tag{39}$$

By defining $\varepsilon_{h,rup} = \beta_\varepsilon \varepsilon_{fu}$ and $v_{s,u} = \alpha_v v_{s,\max}$, then rearranging Eq. (39), the normalized ultimate axial strain can be expressed as:

$$\frac{\varepsilon_{cu,r}}{\varepsilon_{c0}} = \frac{\varepsilon_{h,rup}}{v_{s,u}\varepsilon_{c0}} = \frac{\beta_\varepsilon \varepsilon_{fu}}{\alpha_v v_{s,\max}\varepsilon_{c0}} = \frac{\beta_\varepsilon \rho_\varepsilon}{\alpha_v v_{s,\max}} \tag{40}$$

in which

$$\rho_\varepsilon = \frac{\varepsilon_{fu}}{\varepsilon_{c0}} \tag{41}$$

where α_v is the ratio of $v_{s,u}$ and $v_{s,\max}$; β_ε introduces the ratio of FRP ultimate hoop strain ($\varepsilon_{h,rup}$) and FRP ultimate tensile strain (ε_{fu}). To obtain the α_v, the ratio of $v_{s,u}$ at ${\varepsilon_{cu,r}}^{Exp}$ and $v_{s,\max}$ for 191 test specimens of FFC were simulated by the developed dilation model, and the obtained results are presented in Fig. 12a. By best fitting these results, the following equation was obtained:

$$\alpha_v = 1 - 0.85\rho_{K,f} \geq 0.8 \tag{42}$$

It should be noted that in Eq. (42), for low level of $\rho_{K,f}$ ($\rho_{K,f} \leq 0.015$) (with ${\varepsilon_{cu,r}}^{Exp} < \varepsilon_{c,m}$), the ascending branch α_v versus $\rho_{K,f}$ relation was neglected for the sake of simplification. Then, by using Eq. (42), ${\beta_\varepsilon}^{Exp}$ was calculated as $\alpha_v v_{s,\max} {\varepsilon_{cu,r}}^{Exp} / \varepsilon_{fu}$. Accordingly, the relation of β_ε with f_{c0} was determined as follows (Fig. 12b):

$$\beta_\varepsilon = 1.45 {f_{c0}}^{-0.27} \tag{43}$$

Therefore, with the consideration of $v_{s,\max} = 0.15/\sqrt{\rho_{K,f}}$ (Fig. 9a), replacing Eq. (43) in Eq. (40) leads to:

$$\frac{\varepsilon_{cu,r}}{\varepsilon_{c0}} = 9.67\, f_{c0}{}^{-0.27} \frac{\sqrt{\rho_{K,f}}}{1-0.85\rho_{K,f}} \rho_{\varepsilon} \tag{44}$$

379 In order to simplify Eq. (44), rearranging this equation gives:

$$\frac{\varepsilon_{cu,r}}{X} = \frac{\sqrt{\rho_{K,f}}}{1-0.85\rho_{K,f}} \simeq C_1 \rho_{K,f}{}^{C_2} \tag{45}$$

380 in which $X = 9.67\, f_{c0}{}^{-0.27} \varepsilon_{c0} \rho_{\varepsilon}$, while C_1 and C_2 are the calibration factors, which were determined

381 equal to 1.83 and 0.61, respectively, based on the relation of $\varepsilon_{cu,r}{}^{Exp} \big/ X$ with $\rho_{K,f}$ as demonstrated

382 in Fig. 13c. Accordingly, $\varepsilon_{cu,r}$ can be expressed as:

$$\frac{\varepsilon_{cu,r}}{\varepsilon_{c0}} = 17.7\, f_{c0}{}^{-0.27} \rho_{K,f}{}^{0.61} \rho_{\varepsilon} \geq 1.5 \tag{46}$$

383 The lower bound of 1.5 was considered to limit ultimate axial strain corresponding to unconfined

384 concrete. For the case of FPC, $\varepsilon_{cu,r}$ corresponding to $\varepsilon_{h,rup} = k_{ff}{}^{FPC} \varepsilon_{l,j}$ at the FRP strips can be

385 written as:

$$\varepsilon_{cu,r} = \frac{\varepsilon_{l,j}}{v_{s,u}} = \frac{\varepsilon_{h,rup}}{k_{ff}{}^{FPC} v_{s,u}} \tag{47}$$

386 Rearranging Eq. (38), the normalized ultimate axial strain can be expressed as:

$$\frac{\varepsilon_{cu,r}}{\varepsilon_{c0}} = \frac{\varepsilon_{h,rup}}{k_{ff}{}^{FPC} v_{s,u} \varepsilon_{c0}} = \frac{\beta_{\varepsilon} \rho_{\varepsilon}}{k_{ff}{}^{FPC} \alpha_v v_{s,\max}} = \frac{17.7}{k_{ff}{}^{FPC}} f_{c0}{}^{-0.27} \rho_{K,f}{}^{0.61} \rho_{\varepsilon} \tag{48}$$

387 In order to minimize the complexity of Eq. (48), based on the best-fit with the derived results from

388 135 test specimens of FPC, Eq. (48) was simplified as follows:

$$\frac{\varepsilon_{cu,r}}{\varepsilon_{c0}} = 17.7\gamma_{sf} {f_{c0}}^{-0.27} {\rho_{K,f}}^{0.61} \rho_{\varepsilon} \geq 1.5 \quad (f_{c0} \text{ in MPa}) \tag{49}$$

in which

$$\gamma_{sf} = \frac{\gamma_1}{\gamma_2} \tag{50}$$

$$\gamma_1 = 70{R_f}^3 - 85{R_f}^2 + 33R_f - 2.1 \leq 5 \tag{51}$$

$$\gamma_2 = 1.85 - 0.85\frac{L_{d0}}{D} \tag{52}$$

where γ_{sf}, γ_1 and γ_2 are the calibration parameters determined based on regression analyses as shown in Figs. 12d-e; R_f defines the ratio of the FRP strip distance (s_f) and the column cross-section diameter (D) as presented in Eq. (15). It should be noted that ${\gamma_1}^{Exp}$ and ${\gamma_2}^{Exp}$ were determined based on Eq. (49), as ${\gamma_1}^{Exp} = {\varepsilon_{cu,r}}^{Exp} \Big/ \left(17.7 {f_{c0}}^{-0.27} {\rho_{K,f}}^{0.61} \rho_{\varepsilon} \varepsilon_{c0}\right)$ and ${\gamma_2}^{Exp} = \left(17.7\gamma_1 {f_{c0}}^{-0.27} {\rho_{K,f}}^{0.61} \rho_{\varepsilon} \varepsilon_{c0}\right) \Big/ {\varepsilon_{cu,r}}^{Exp}$, respectively.

For the case of FPC with a large R_f, the failure mode is prominently overwhelmed by the concrete crushing within the damage length zone. Wang *et al.* [44] experimentally evidenced that for the case of $R_f \geq 1$, the failure mode would be as concrete crushing with no FRP rupture (Fig. 11e). It can be attributed to the difference in Poisson's ratio at the critical section experiencing a major damage and at the mid-plane of FRP strip in which concrete expansion could not be enough to increase FRP hoop strain to experience the rupture. Accordingly, for FPC with a large R_f, the application of Eq. (49), predicting ultimate axial strain corresponding to FRP rupture ($\varepsilon_{cu,r}$), might lead to overestimation in terms of deformability, considering the fact that FPC would behave

similar to unconfined concrete. Shayanfar *et al.* [23] developed a new methodology to predict ultimate axial strain (ε_{cu}) of FPC formulating the possibility of concrete crushing failure mode ($\varepsilon_{cu,c}{}^{FPC}$), in addition to FRP rupture ($\varepsilon_{cu,r}$), leading to $\varepsilon_{cu}=\min\left(\varepsilon_{cu,r},\varepsilon_{cu,c}{}^{FPC}\right)$. Since all test specimens of FFC with $R_f \le 0.75$, available in the test database, experienced FRP rupture failure mode, the application of $\varepsilon_{cu,r}$ in Eq. (49) for estimation of ε_{cu} would be reasonable. However, for the case of $R_f \ge 0.75$, based on Shayanfar *et al.* [23], an upper bound needs to be introduced to restrain ultimate axial strain by considering the possibility of concrete crushing. Even though the application of FPC with $R_f \ge 0.75$ is not allowed in the real strengthening cases, in the present study, ε_{cu} for $R_f \ge 0.75$ was assumed to be equal to $\varepsilon_{cu,r}$ and $1.5\varepsilon_{c0}$ (ultimate axial strain of unconfined concrete) corresponding to $R_f = 0.75$ and $R_f \ge 1$ (considered as unconfined concrete), respectively. Consequently, using a linear function, $\varepsilon_{cu,c}{}^{FPC}$ can be as determined as:

$$\frac{\varepsilon_{cu,c}{}^{FPC}}{\varepsilon_{c0}} = 1.5 + 4\left(\frac{\varepsilon_{cu,r}}{\varepsilon_{c0}} - 1.5\right)\left(1 - R_f\right) \ge 1.5 \tag{53}$$

In Fig. 12f, ultimate axial strains of FPC obtained from the developed model were compared with those of the experimental studies. It can be evidenced that the proposed approach is capable of calculating ε_{cu} ($\min\left(\varepsilon_{cu,r},\varepsilon_{cu,c}{}^{FPC}\right)$) with an acceptable agreement with the experimental counterparts.

7- Verification

In this section, the reliability of the proposed confinement model in simulating the experimental counterparts is addressed. In Fig. 13, a flowchart for calculating axial stress-strain curve of FRP fully/partially confined concrete columns is presented. As can be seen, the effectiveness of FRP

422 confining system can be easily determined through following the proposed incremental procedure.
423 In order to appropriately assess the model, in addition to global axial response, its capability in
424 predicting the dilation response is also examined. Zeng *et al.* [5] conducted an experimental study
425 on fully/partially FRP confined circular concrete with different s_f , n_f and confinement types of
426 full and partial systems. The test specimens had a diameter of 150 mm with a height of 300 mm.
427 The compressive strength of unconfined cylindrical concrete was 23.4 MPa. The values of
428 thickness, tensile elastic modulus and rupture strain of FRP strips were reported as 0.167 mm,
429 249.1 GPa and 1.66%, respectively. Complete detailed of the test specimens can be found from
430 Zeng *et al.* [5]. The axial and dilation responses of the test specimens reported by the experiment
431 and obtained from the proposed model are compared in Fig. 14. As can be observed, the proposed
432 model has a good predictive performance, with a slightly conservative tendency to predict not only
433 the global axial stress-strain curves of the test specimens with full/partial confinement systems,
434 but also experimental axial stress versus lateral strain.

435 For further examination of the model capability in predicting axial response, In Fig. 15, axial
436 responses obtained from the analytical model are compared to those experimentally measured by
437 Zeng *et al.* [43], Shan *et al.* [46] and Gue *et al.* [8], which are the larger dimension specimens
438 found in the database for the assessment of the performance of the developed model in predicting
439 their axial stress-strain response. As can be seen, the predictions are in an acceptable agreement
440 with the global axial stress-strain curve of the experimental FFC/FPC specimens. Supplementary
441 results regarding the validations of the developed model in simulating axial behavior of FFC and
442 FPC can be found, respectively, in Figs. B1 and B2 in Appendix B.

Fig. 16 evaluated the predictive performance of the developed confinement model, in the estimation of ultimate axial stress and strain (f_{cu}^{Exp} and ε_{cu}^{Exp}) of FFC and FPC, compared to that of existing models recommended by *fib* [25], CNR DT 200/2004 [26] and ACI 440.2R-17 [27], which can be found in Appendix A.

As can be seen, for the case of FFC, the proposed model provided the most accurate and uniform predictions of f_{cu}^{Exp} with the values of mean, SD (standard deviation) and MAPE (mean absolute percentage error which is expressed as $MAPE = \frac{1}{N}\sum_{1}^{N}\left|1 - f_{cu}^{Ana} / f_{cu}^{Exp}\right|$ where N is the total number of the test data) as 0.99, 0.15 and 0.12, respectively. ACI 440.2R-17 [27] presented a slight underestimation of the experimental counterpart (mean = 0.89), with the values of SD and MAPE as 0.15 and 0.15. On the other hand, for the case of FPC, CNR DT 200/2004 [26] demonstrated the most accurate model, with the values of mean, SD and MAPE as 1.00, 0.12 and 0.10, respectively. The predictive performance of the proposed model in predicting f_{cu}^{Exp} is virtually identical to CNR DT 200/2004 [26], but with slightly more SD equal to 0.13.

For the case of ε_{cu}^{Exp}, *fib* [25] and CNR DT 200/2004 [26] conservatively predicted the experimental counterparts, even though ACI 440.2R-17 [27] seems to provide better estimations of ultimate axial strain for the case of FFC, non-conservative results for some test specimens of FPC are obtained which slightly overwhelm its reliability evaluation. The predictive performance of Eq. (48) confirmed its reliability to predict the experimental axial strain with sufficient accuracy demonstrated by the relative statistical values for the both cases of FFC and FPC.

As demonstrated in Figs. 14-16, it can be concluded that the developed model conducted in the present study is sufficiently capable of predicting not only the global axial stress-strain relationship of FFC/FPC, but also the ultimate conditions (f_{cu}^{Exp} and ε_{cu}^{Exp}).

9-Summary and conclusions

In the present study, a new unified confinement model applicable to different confinement scenarios including circular cross-sections concrete columns with full and partial confining strategies was proposed. To simulate the axial stress versus strain curve, a new strength model is proposed addressing the relation of axial stress and confinement pressure during axial loading, whose calibration was based on an extensive set of test results. For formulating the influence of concrete expansion distribution in the calculation of confinement pressure, Shayanfar *et al.* [23]'s model is extended to be applicable to FFC as a function of confinement stiffness, along with some refinements for the case of FPC. In this model, the concrete lateral expansibility was addressed as a main function of confinement stiffness (I_f) and also s_f / L_{d0} for the case of FPC. A new expression is subsequently developed to estimate ultimate axial strain of FFC/FPC with a combination of theoretical basis and experimental observations. Lastly, the predictive performance of the developed confinement model was assessed through analytically simulating experimental counterparts. The comparison between the analytical model and experimental counterparts demonstrated that global axial stress-strain curves simulated by the proposed confinement model are in good agreement with those registered experimentally in available literature, and provides better predictions in terms of ultimate axial stress/strain than the formulations proposed by design standards. The authors are working on the extension of the present formulation in order to be applicable to non-circular cross section columns, where the non-homogeneous concrete

expansibility at the cross-section level must be also considered by taking into account the influence of the sectional corner radius.

Data Availability Statement

All data and models related to the present study could be available from the corresponding author upon rational request.

Acknowledgments

This study is a part of the project ‘‘StreColesf_Innovative technique using effectively composite materials for the strengthening of rectangular cross section reinforced concrete columns exposed to seismic loadings and fire’’, with the reference POCI-01-0145-FEDER-029485. The firs author also acknowledges the support provided by FCT PhD individual fellowship 2019 with the reference of “SFRH/BD/148002/2019”.

References

[1] De Oliveira DS, Raiz V, Carrazedo. Experimental study on normal-strength, high-strength and ultrahigh-strength concrete confined by carbon and glass FRP laminates. J Compos Constr 2019;23(1):04018072.

[2] Lim JC, Ozbakkaloglu T. Lateral strain-to-axial strain relationship of confined concrete. J Struct Eng 2014;141(5):04014141.

[3] Lim JC, Ozbakkaloglu T. Unified stress-strain model for FRP and actively confined normal strength and high-strength concrete. J Compos Constr 2014;19(4):04014072.

[4] Lim JC, Ozbakkaloglu T. Hoop strains in FRP-confined concrete columns: experimental observations. Mater Struct 2014;48(9):2839-2854.

[5] Zeng JJ, Guo YC, Gao WY, Chen WP, Li LJ. Stress-strain behavior of concrete in circular concrete columns partially wrapped with FRP strips. Compos Struct 2018;200:810-828.

[6] Barros JA, Ferreira DR. Assessing the efficiency of CFRP discrete confinement systems for concrete cylinders. J Compos Constr 2008;12(2):134-148.

[7] Zeng JJ, Guo YC, Li L, Chen W. Behavior and three-dimensional finite element modeling of circular concrete columns partially wrapped with FRP strips. Polymers 2018;10(3):253.

[8] Guo YC, Gao WY, Zeng JJ, Duan ZJ, Ni XY, Peng KD. Compressive behavior of FRP ring-confined concrete in circular columns: Effects of specimen size and a new design-oriented stress-strain model. Constr Build Mater 2019;201:350-368.

[9] Guo YC, Xiao SH, Luo JW, Ye YY, Zeng JJ. Confined Concrete in Fiber-Reinforced Polymer Partially Wrapped Square Columns: Axial Compressive Behavior and Strain Distributions by a Particle Image Velocimetry Sensing Technique. Sensors 2018;18(12):4118.

[10] Janwaen W, Barros JA, Costa IG. A new strengthening technique for increasing the load carrying capacity of rectangular reinforced concrete columns subjected to axial compressive loading. Compos Part B Eng 2019;158:67-81.

[11] Janwaen W, Barros JA, Costa IG. New Hybrid FRP Strengthening Technique for Rectangular RC Columns Subjected to Eccentric Compressive Loading. J Compos Constr 2020;24(5):04020043.

[12] Jiang T, Teng JG. Analysis-oriented stress–strain models for FRP–confined concrete. Eng Struct 2007;29(11):2968-2986.

[13] Teng J, Huang YL, Lam L, Ye LP. Theoretical model for fiber-reinforced polymer-confined concrete. J Compos Constr 2007;11(2):201-210.

[14] Teng JG, Lin G, Yu T. Analysis-oriented stress-strain model for concrete under combined FRP-steel confinement. J Compos Constr 2015;19(5):04014084.

[15] Lim JC, Ozbakkaloglu T. Stress–strain model for normal-and light-weight concretes under uniaxial and triaxial compression. Constr Build Mater 2014;71:492-509.

[16] Popovics S. A numerical approach to the complete stress-strain curve of concrete. Cement and concrete research 1973;3(5):583-599.

[17] Lin S, Zhao YG, Li J, Lu ZH. Confining Stress Path-Based Compressive Strength Model of Axially Loaded FRP-Confined Columns. J Compos Constr 2020;25(1):04020077.

536 [18] Yang JQ, Feng, P. Analysis-oriented models for FRP-confined concrete: 3D interpretation and general
537 methodology. Eng Struct 2020;216:110749.

538 [19] Zhao YG, Lin S, Lu ZH, Saito T, He L. Loading paths of confined concrete in circular concrete loaded
539 CFT stub columns subjected to axial compression. Eng Struct 2018;156:21-31.
540 [20] Wu YF, Wei Y. Stress–Strain Modeling of Concrete Columns with Localized Failure: An Analytical
541 Study. J Compos Constr 2016;20(3):04015071.

542 [21] Wei Y, Wu YF. Experimental study of concrete columns with localized failure. J Compos Constr
543 2016:20(5):04016032.

544 [22] Fallahpour A, Nguyen GD, Vincent T, Ozbakkaloglu T. Investigation of the compressive behavior and
545 failure modes of unconfined and FRP-confined concrete using digital image correlation. Compos
546 Struct 2020;252:112642.
547 [23] Shayanfar J, Rezazadeh M, Barros JA. Analytical model to predict dilation behavior of FRP confined
548 circular concrete columns subjected to axial compressive loading. J Compos Constr
549 2020;24(6):04020071.

550 [24] Mander JB, Priestley MJ, Park R. Theoretical stress-strain model for confined concrete. J Struct Eng
551 1988;114(8):1804-1826.

552 [25] Fib Bulletin 14. Externally bonded FRP reinforcement for RC structures. International Federation for
553 Structural Concrete 2001.

554 [26] CNR-DT 200. Guide for the design and construction of externally bonded FRP systems for
555 strengthening existing structures. Italian National Research Council 2004.

556 [27] ACI 440.2R-17. Guide for the design and construction of externally bonded FRP systems for
557 strengthening concrete structures; American Concrete Institute (ACI): Farmington Hills MI USA
558 2017.

559 [28] Teng JG, Jiang T, Lam L, Luo YZ. Refinement of a design-oriented stress–strain model for FRP-
560 confined concrete. J Compos Constr 2010;13(4):269-278.

561 [29] Karthik MM, Mander JB. Stress-block parameters for unconfined and confined concrete based on a
562 unified stress-strain model. J Struct Eng 2010;137(2):270-273.

563 [30] Wang LM, Wu YF. Effect of corner radius on the performance of CFRP-confined square concrete
564 columns: Test. Eng Struct 2008;30(2):493-505.

565 [31] Eid R, Roy N, Paultre P. Normal-and high-strength concrete circular elements wrapped with FRP
566 composites. J Compos Constr 2009;13(2):113-124.

567 [32] Shayanfar J, Rezazadeh M, Barros JA, Ramezansefat H. A new dilation model for FRP fully/partially
568 confined concrete column under axial loading. The 3RD RILEM Spring Convention 2020
569 Ambitioning a Sustainable Future for Built Environment: Comprehensive Strategies for
570 Unprecedented Challenges, Guimarães Portugal 2020.

571 [33] Lertsrisakulrat T, Watanabe K, Matsuo M, Niwa, J. Experimental study on parameters in localization
572 of concrete subjected to compression. J Mater Concr Struct Pavements 2001;50(669):309–321.

573 [34] Candappa DC, Sanjayan JG, Setunge S. Complete triaxial stress-strain curves of high-strength
574 concrete. Journal of Materials in Civil Engineering 2001;13(3):209-215.

575 [35] Rochette P, Labossiere P. Axial testing of rectangular column models confined with composites. J
576 Compos Constr 2000;4(3):129-136.

577 [36] Shehata IA, Carneiro LA, Shehata LC. Strength of short concrete columns confined with CFRP
578 sheets. Mater Struct 2002;35(1):50-58.

579 [37] Teng JG, Lam L. Compressive behavior of carbon fiber reinforced polymer-confined concrete in
580 elliptical columns. J Struct Eng 2002;128(12):1535-1543.

581 [38] Xiao Y, Wu H. Compressive behavior of concrete confined by various types of FRP composite
582 jackets. J Reinforc Plast Compos 2003;22(13):1187-1201.

583 [39] Berthet JF, Ferrier E, Hamelin P. Compressive behavior of concrete externally confined by composite
584 jackets. Part A: experimental study. Constr Build Mater 2005;19(3):223-232.

585 [40] Wang F, Wu HL. Size effect of concrete short columns confined with aramid FRP jackets. J Compos
586 Constr 2011; 15(4), 535-544.

587 [41] Benzaid R, Mesbah HA. Circular and square concrete columns externally confined by CFRP
588 composite: experimental investigation and effective strength models. Fiber Reinforced Polymers–
589 The Technology Applied for Concrete Repair 2013;167-201.

590 [42] Vincent T, Ozbakkaloglu T. Compressive behavior of prestressed high-strength concrete-filled aramid
591 FRP tube columns: Experimental observations. J Compos Constr 2015;19(6):04015003.

592 [43] Zeng JJ, Guo YC, Gao WY, Li JZ, Xie JH. Behavior of partially and fully FRP-confined circularized
593 square columns under axial compression. Constr Build Mater 2017;152:319-332.

[44] Wang W, Sheikh MN, Al-Baali AQ, Hadi MN. Compressive behaviour of partially FRP confined concrete: Experimental observations and assessment of the stress-strain models. Constr Build Mater 2018;192, 785-797.

[45] Suon S, Saleem S, Pimanmas A. Compressive behavior of basalt FRP-confined circular and non-circular concrete specimens. Constr Build Mater 2019;19, :85-103.

[46] Shan B, Gui FC, Monti G, Xiao Y (2019). Effectiveness of CFRP confinement and compressive strength of square concrete columns. J Compos Constr 2019 23(6):04019043.

[47] Carreira and Chu (1985). Stress-strain relationship for plain concrete in compression. In Journal Proceedings 1985;82(6):797–804.

List of Tables

List of Figures

Fig. 9. a) Variation of the experimental dilation results with $\rho_{K,f}$; b) Predictive performance of Eq. (28)

Fig. 10. Test data and regression equations for: a) R_1, and b) R_2

Fig. 11. Failure mechanisms of FRP confined concrete based on the experimental studies conducted by a) Suon *et al.* [45]; b) Zeng *et al.* [43]; c, d) Zeng *et al.* [5]; e) Wang *et al.* [44]

Fig. 12. Comparison of experimental results and analytical models

Fig. 13. A flowchart for calculating the characteristics of FFC/FPC

Fig. 14. Analytical analysis versus experimental results for the FRP fully/partially confined specimens tested by Zeng *et al.* [5]

Fig. 15. Analytical analysis versus experimental results for FFC/FPC specimens tested by Zeng *et al.* [43], Shan *et al.* [46], and Gue *et al.* [8]

Fig. 16. Comparison of experimental results and analytical models

Fig. B.1. Analytical analyses versus experimental results for FFC specimens tested by Lim and Ozbakkaloglu [4]

Fig. B.2. Analytical analysis versus experimental results for FPC specimens tested by Barros and Ferreira [6], Zeng *et al.* [7] and Gue *et al.* [8]

Appendix A

In this section, a brief description of the confinement models recommended by fib [25], CNR DT 200/2004 [26] and ACI 440.2R-17 [27] will be introduced for predicting the ultimate axial strain and the ultimate axial stress of concrete.

***fib* [25]**

$$\frac{f_{cu}}{f_{c0}} = 0.3 + 3\sqrt{\frac{f_{l,eff}}{f_{c0}}} \tag{A -1}$$

$$\frac{\varepsilon_{cu}}{\varepsilon_{c0}} = 2 + 1.25\frac{E_c\varepsilon_{h,rup}}{f_{c0}}\sqrt{\frac{f_{l,eff}}{f_{c0}}} \tag{A-2}$$

CNR DT 200/2004 [26]

$$\frac{f_{cu}}{f_{c0}} = 1 + 2.6\left(\frac{f_{l,eff}}{f_{c0}}\right)^{\frac{2}{3}} \tag{A-3}$$

$$\frac{\varepsilon_{cu}}{\varepsilon_{c0}} = 0.0035 + 0.015\sqrt{\frac{f_{l,eff}}{f_{c0}}} \tag{A-4}$$

ACI 440.2R-17 [27]

$$\frac{f_{cu}}{f_{c0}} = 1 + 3.3\psi_f \frac{f_{l,eff}}{f_{c0}} \tag{A-5}$$

$$\frac{\varepsilon_{cu}}{\varepsilon_{c0}} = 1.75 + 12\frac{f_{l,eff}}{f_{c0}}\left(\frac{\varepsilon_{h,rup}}{\varepsilon_{c0}}\right)^{0.45} \tag{A-6}$$

where E_c is the concrete modulus elasticity; $\varepsilon_{h,rup}$ is the effective hoop strain at FRP rupture; ψ_f is the additional reduction factor, equal to 0.95; $f_{l,eff}$ defines the effective confinement pressure of FPC, recommended by

$$f_{l,eff} = k_{v,f} f_{l,f} = \frac{1}{2} k_{v,f} \rho_f E_f \varepsilon_{h,rup} \tag{A-7}$$

in which

$$\varepsilon_{h,rup} = \beta_\varepsilon \varepsilon_{fu} \tag{A-8}$$

$$k_{v,f} = \left(1 - \frac{s_f}{2D}\right)^2 \tag{A-9}$$

where ρ_f is the FRP volumetric ratio; E_f is the FRP modulus elasticity; $k_{v,f}$ is the confinement efficiency factor; β_ε is FRP efficiency factor; and ε_{fu} is the ultimate FRP tensile strain.

678

679 **Appendix B**

680 The axial and dilation responses of the test specimens of FFC conducted by Lim and Ozbakkaloglu
681 [4] and FPC tested by Barros and Ferreira [6], Zeng *et al.* [7] and Gue *et al.* [8] are compared with
682 those obtained from the proposed model in Figs. B.1 and B.2, respectively.

683

684

685

686

Fig. 1.

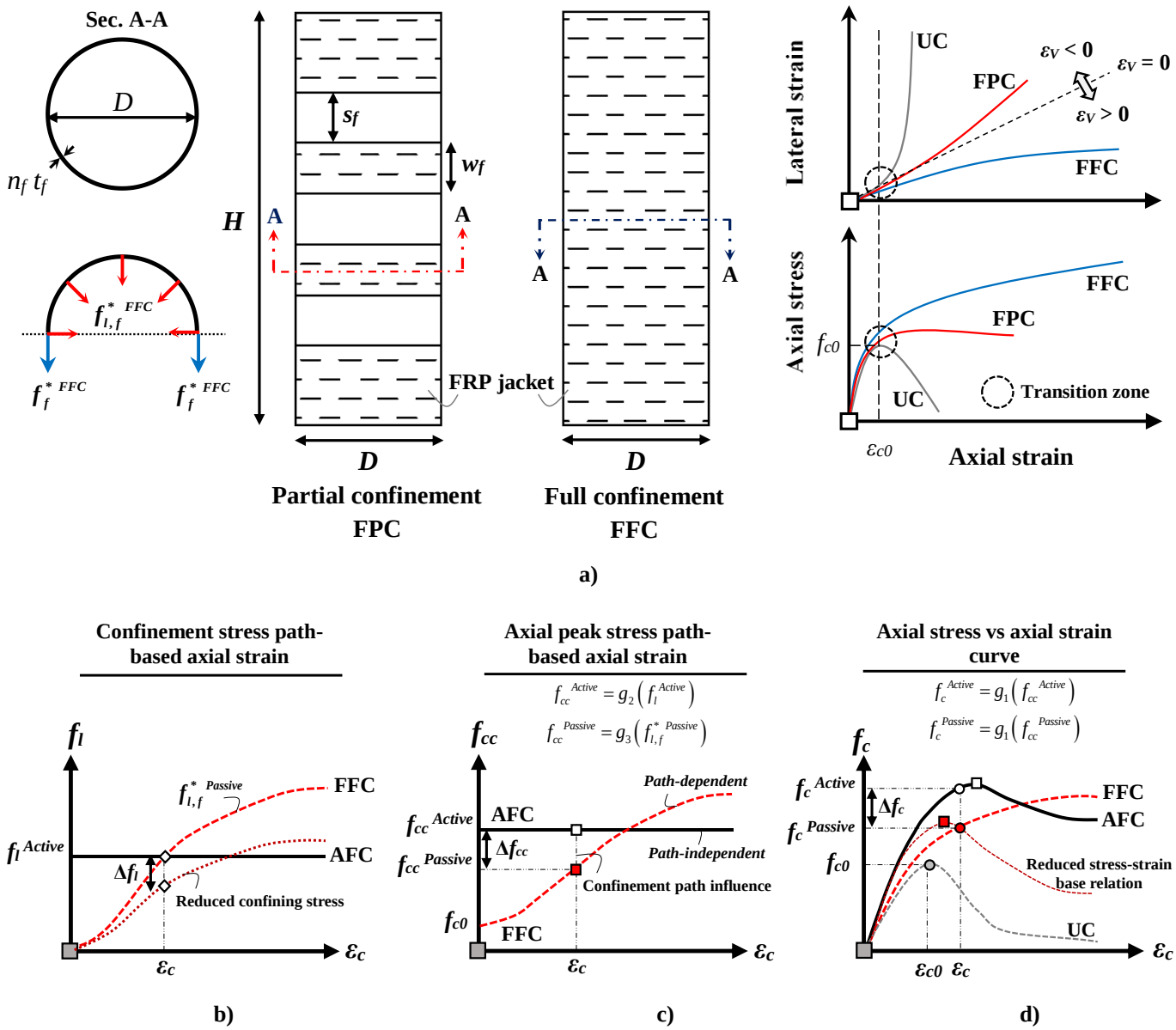

Fig. 1. a) Different confinement configurations; b) Confinement pressure paths of AFC and FFC; c) Peak axial stress vs axial strain; c) Different axial responses of AFC and FFC

Note: UC: unconfined concrete columns; **FFC**: FRP fully confined concrete columns; **FPC**: FRP partially confined concrete columns; **AFC**: Actively confined concrete columns; ε_V defines the concrete volumetric strain (negative value means specimen's volume increase)

Fig. 2.

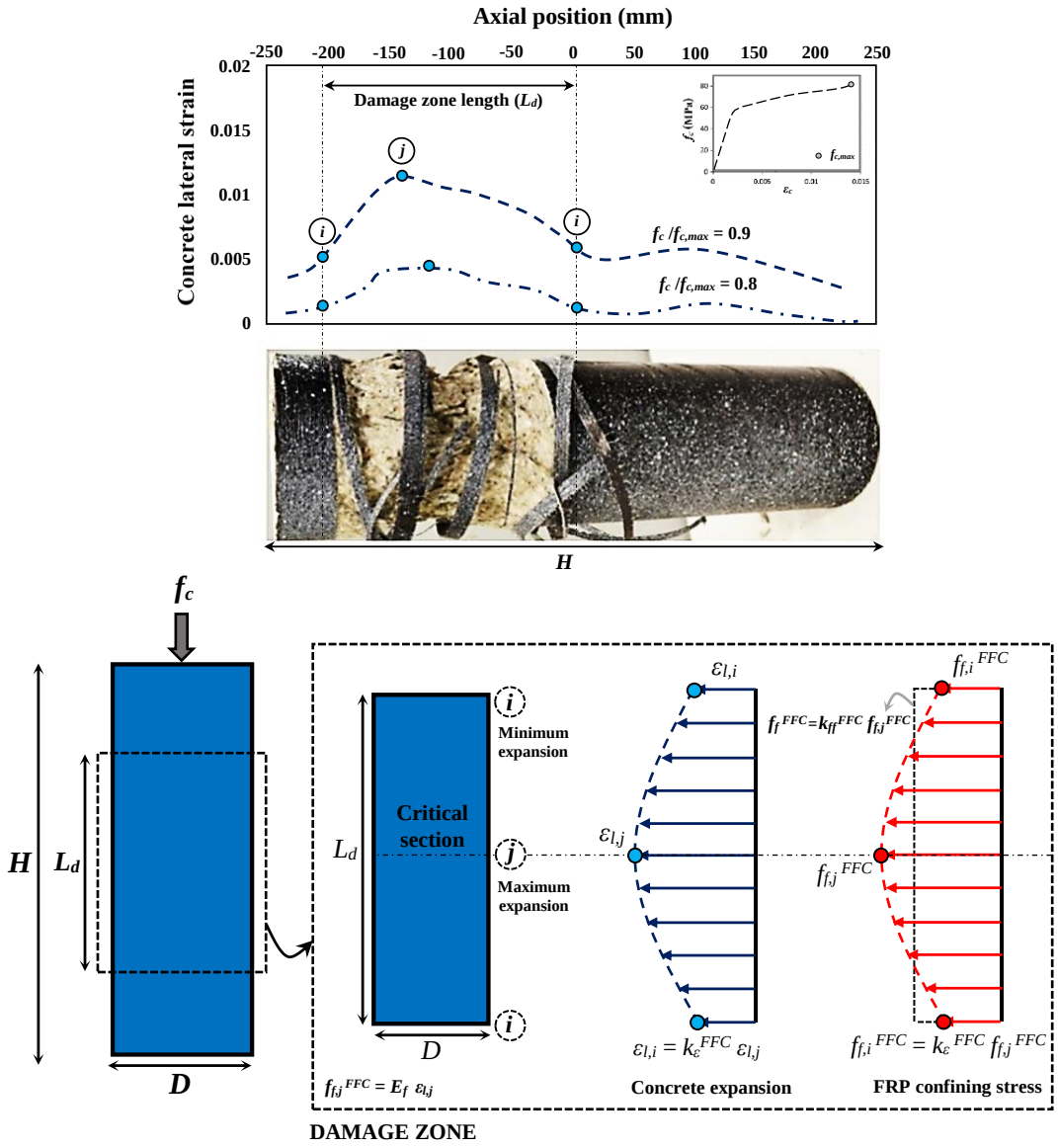

Fig. 2. Distribution of concrete lateral expansion and FRP confining stress

Fig. 3.

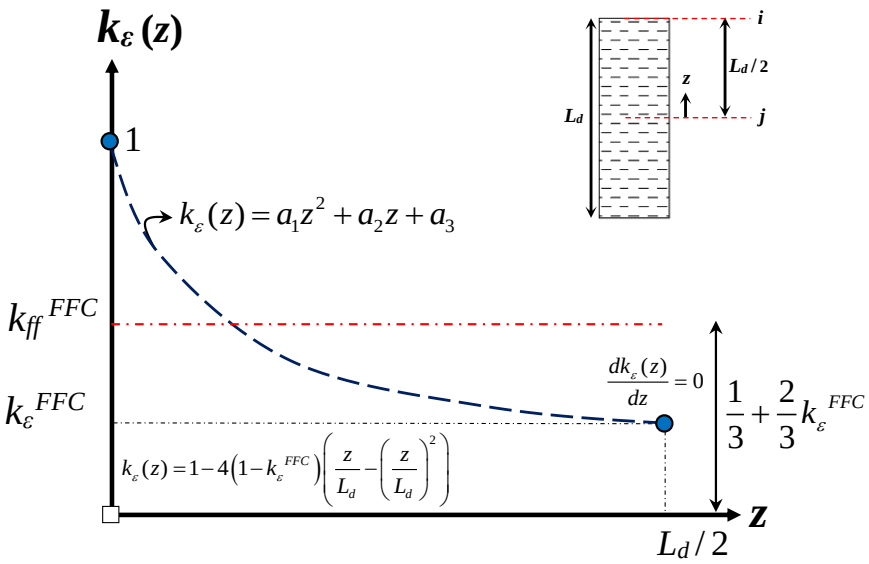

Fig. 3. Distribution $k_\varepsilon(z)$ along $L_d/2$

Fig. 4.

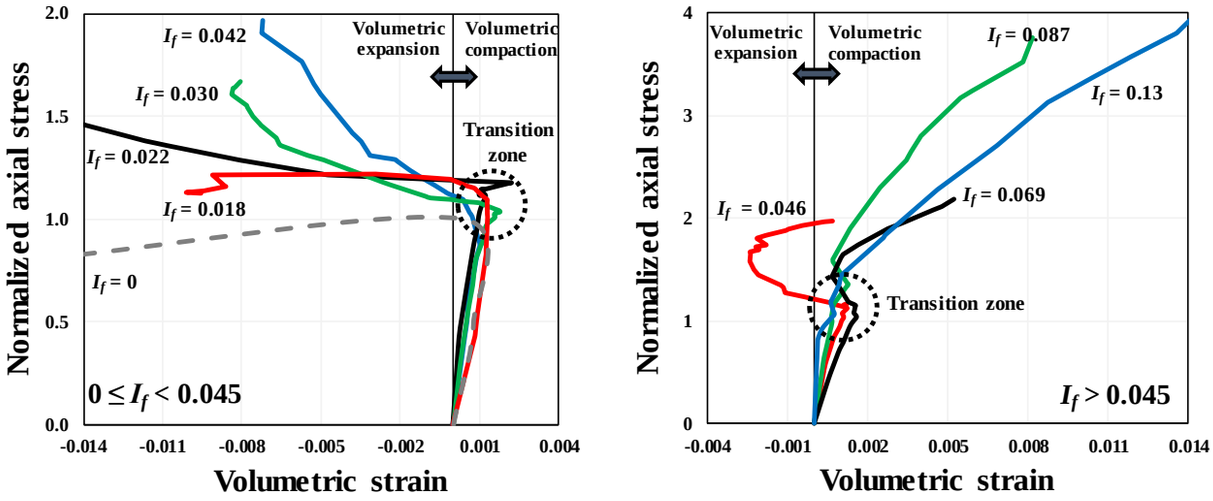

Fig. 4. Normalized axial stress vs volumetric strain

Note: Experimental results from [4, 5, 30, 31]

Fig. 5.

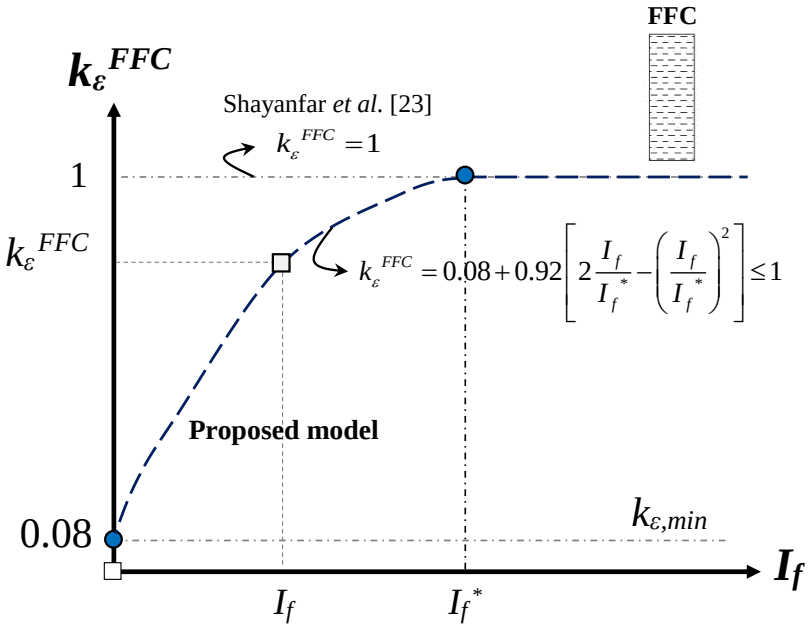

Fig. 5. k_ε^{FFC} versus I_f relation

Fig. 6.

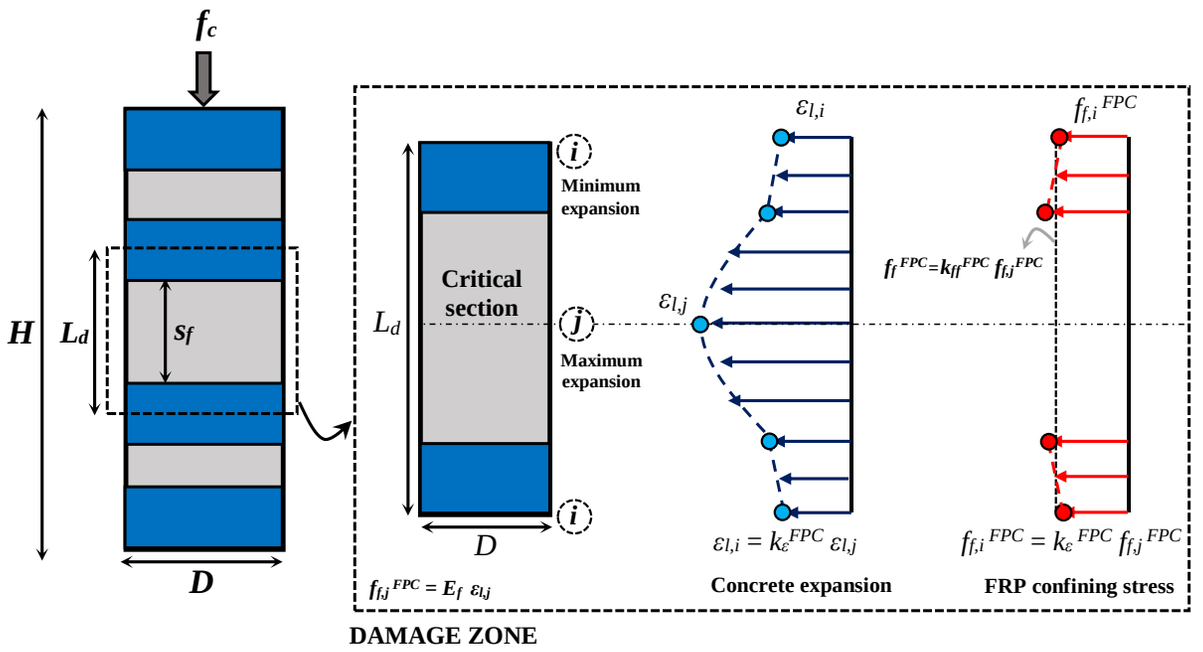

Fig. 6. Distributions of concrete lateral expansion and FRP confining stress for FPC

Fig. 7.

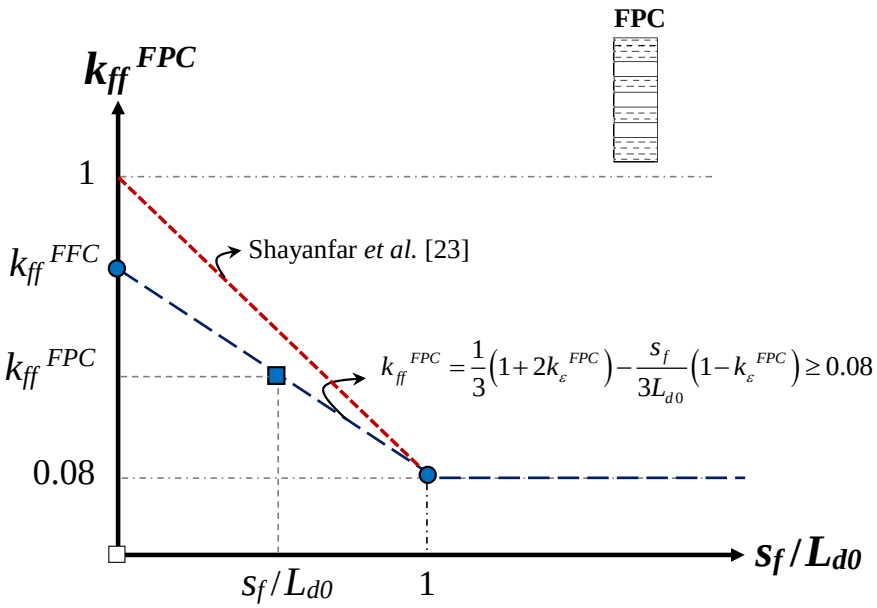

Fig. 7. k_{ff}^{FPC} versus s_f / L_{d0} relation

Fig. 8.

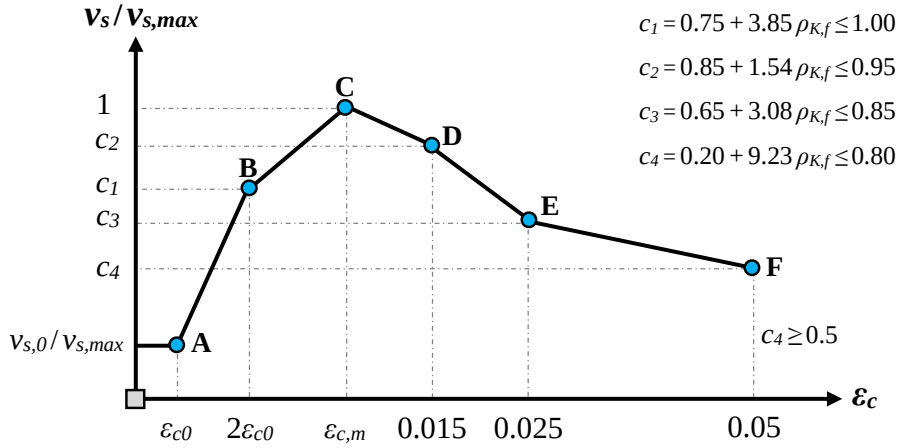

Fig. 8. $v_s / v_{s,max}$ and ε_c relation (redrawn from Shayanfar *et al.* [23])

Fig. 9.

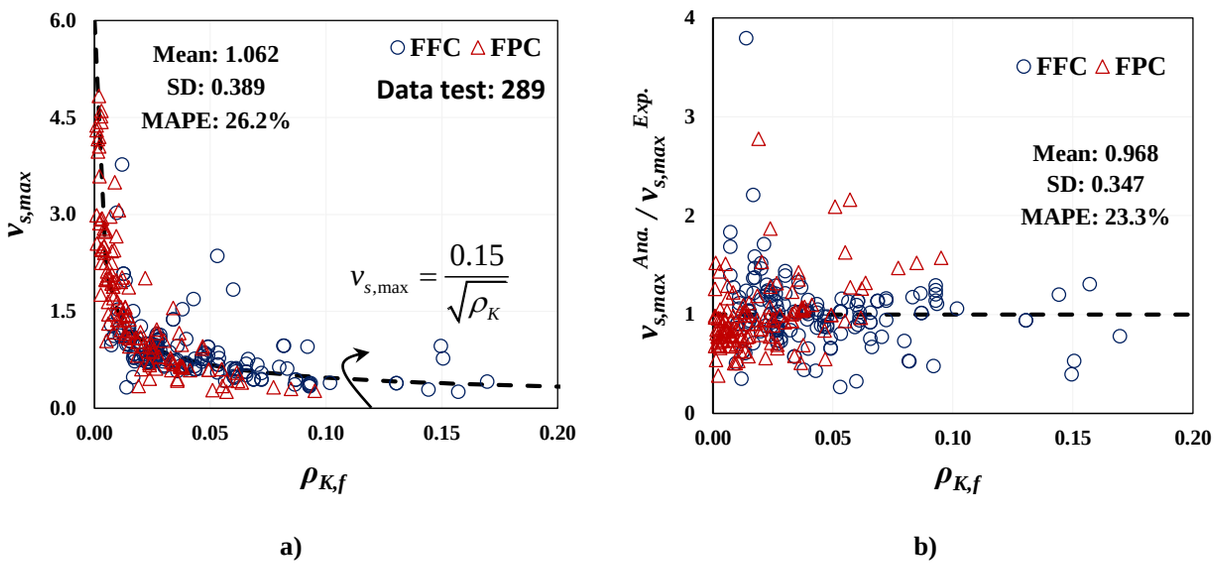

Fig. 9. a) Variation of the experimental dilation results with $\rho_{K,f}$; b) Predictive performance of Eq. (28)

Fig. 10.

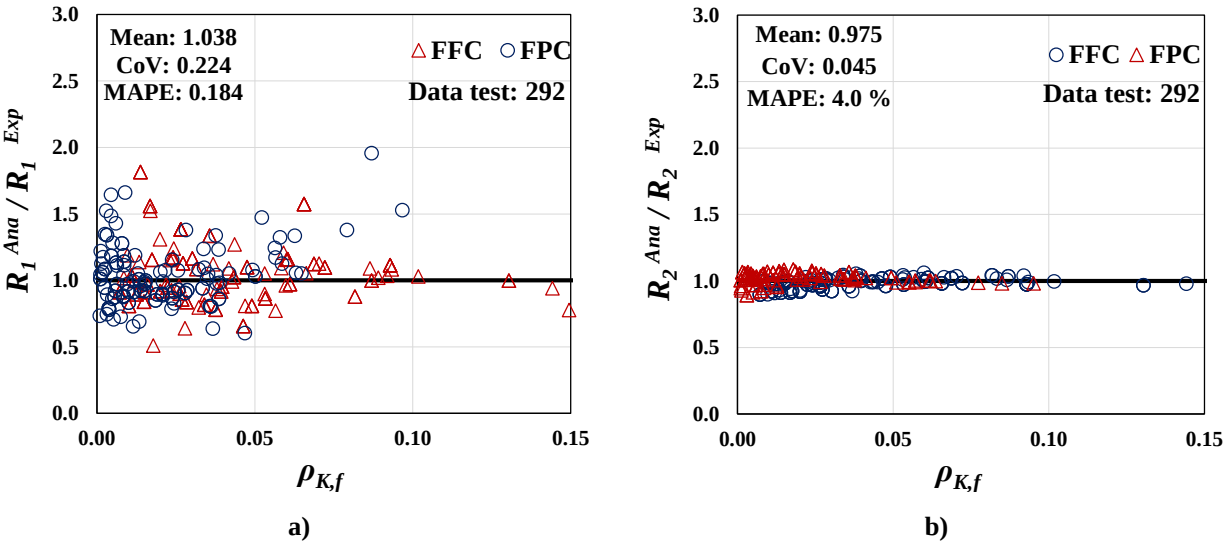

Fig. 10. Test data and regression equations for: a) R_1, and b) R_2

Fig. 11.

$R_f = 0$ $R_f = 0.13$ $R_f = 0.36$ $R_f = 0.65$ $R_f = 1$

FRP rupture **FRP rupture and concrete crushing** **concrete crushing**

a) **b)** **c)** **d)** **e)**

Fig. 11. Failure mechanisms of FRP confined concrete based on the experimental studies conducted by a) Suon *et al.* [45]; b) Zeng *et al.* [43]; c, d) Zeng *et al.* [5]; e) Wang *et al.* [44]

Fig. 12.

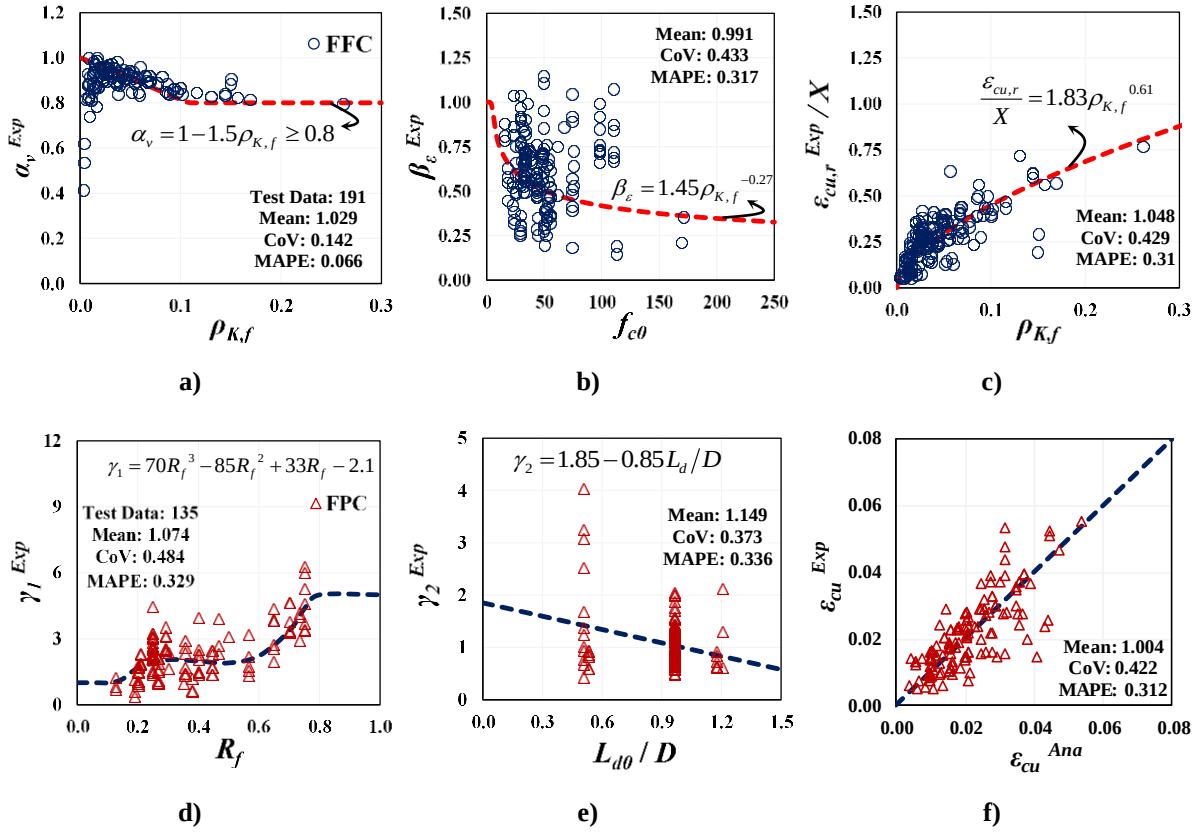

Fig. 12. Comparison of experimental results and analytical models

Fig. 13.

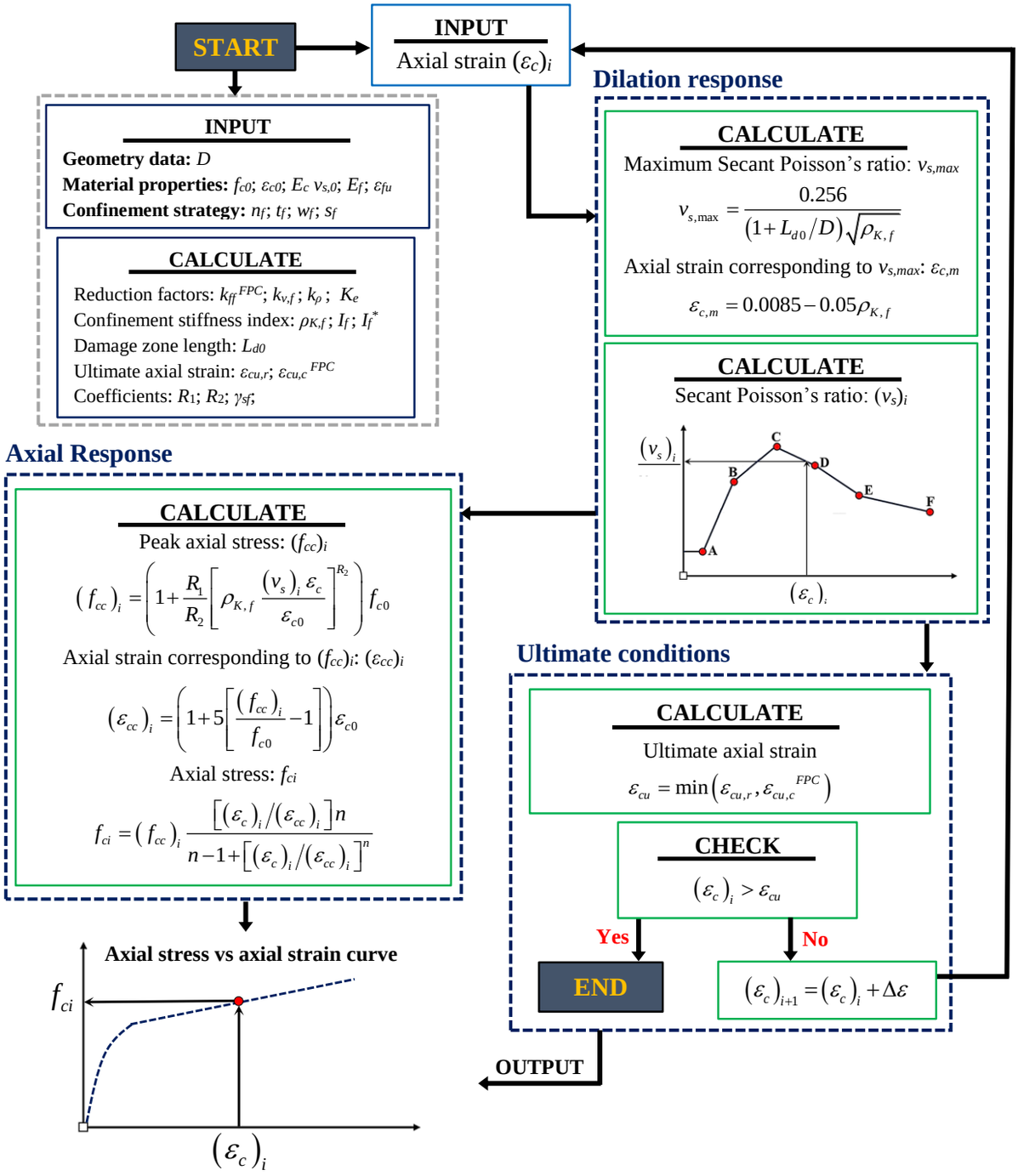

Fig. 13. A flowchart for calculating the characteristics of FFC/FPC

Fig. 14.

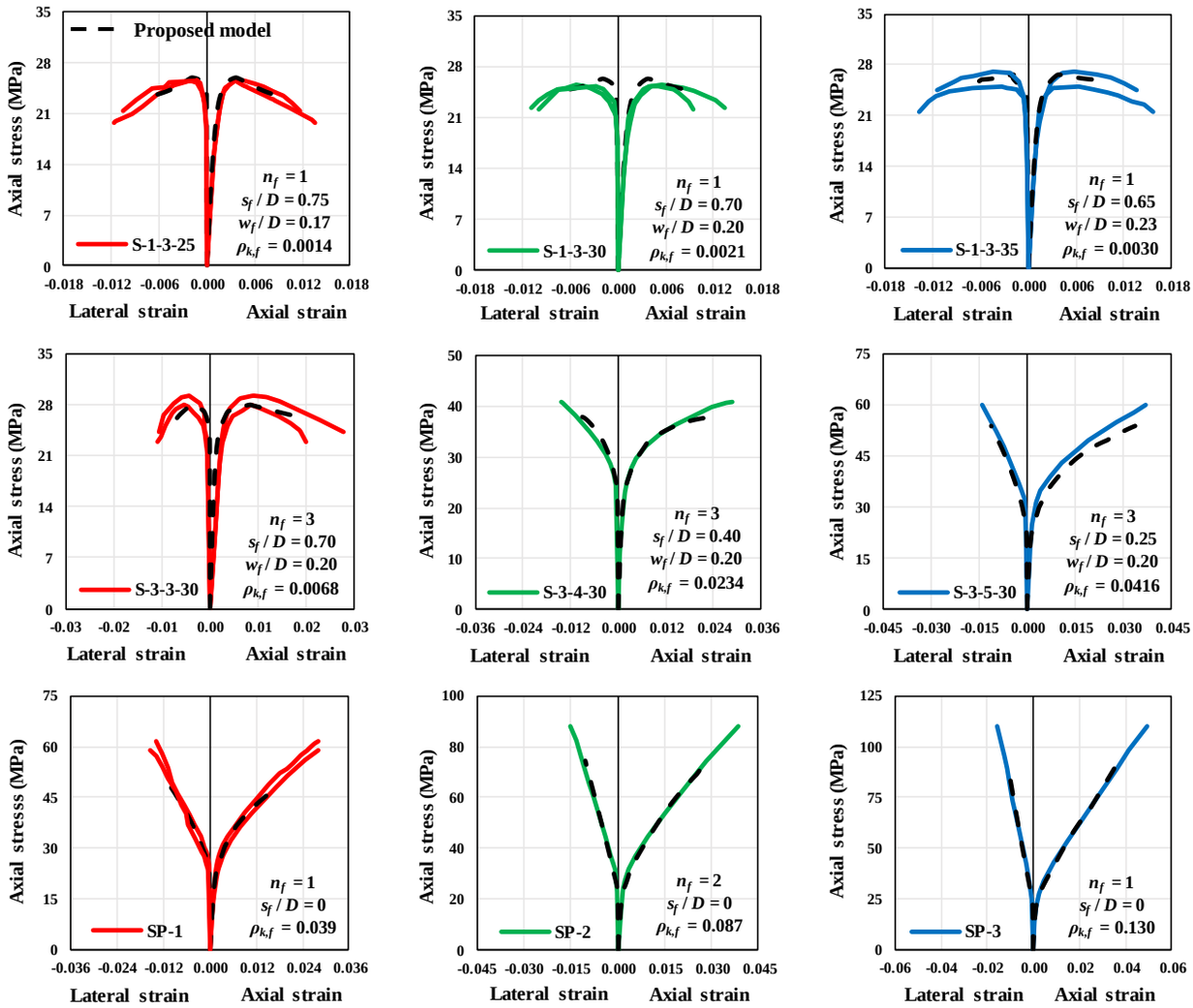

Fig. 14. Analytical analysis versus experimental results for the FRP fully/partially confined specimens tested by Zeng *et al.* [5]

Fig. 15.

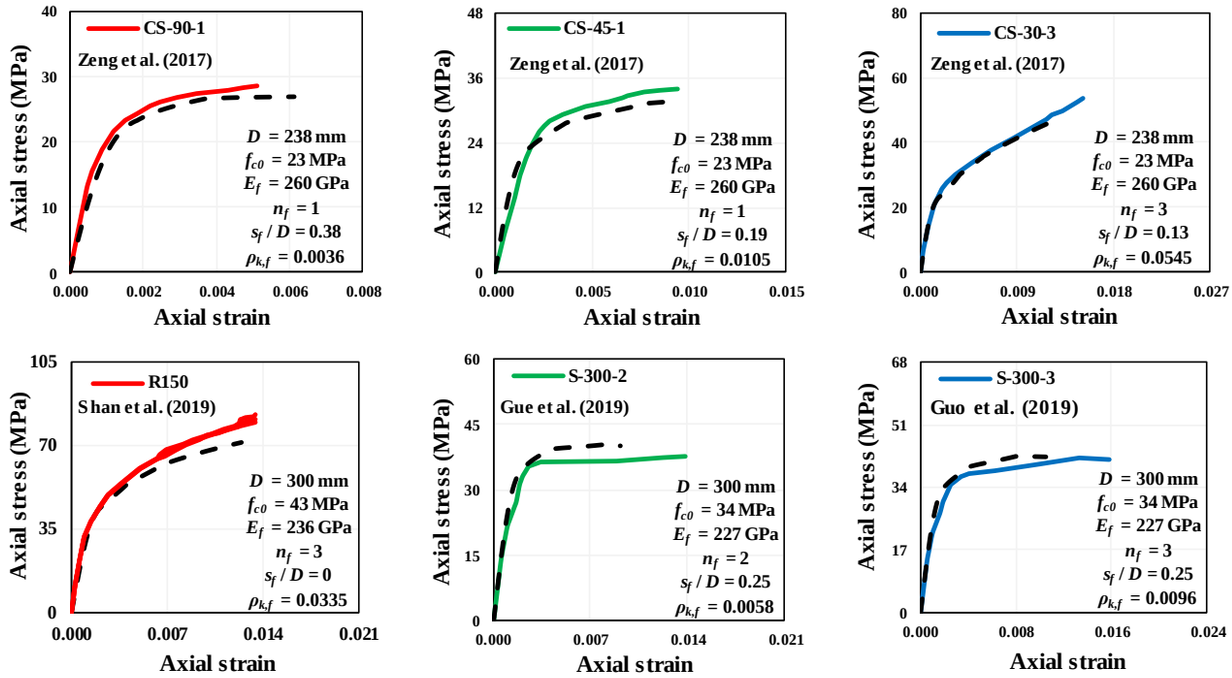

Fig. 15. Analytical analysis versus experimental results for FFC/FPC specimens tested by Zeng *et al.* [43], Shan et al. [46], and Gue et al. [8];

Fig. 16.

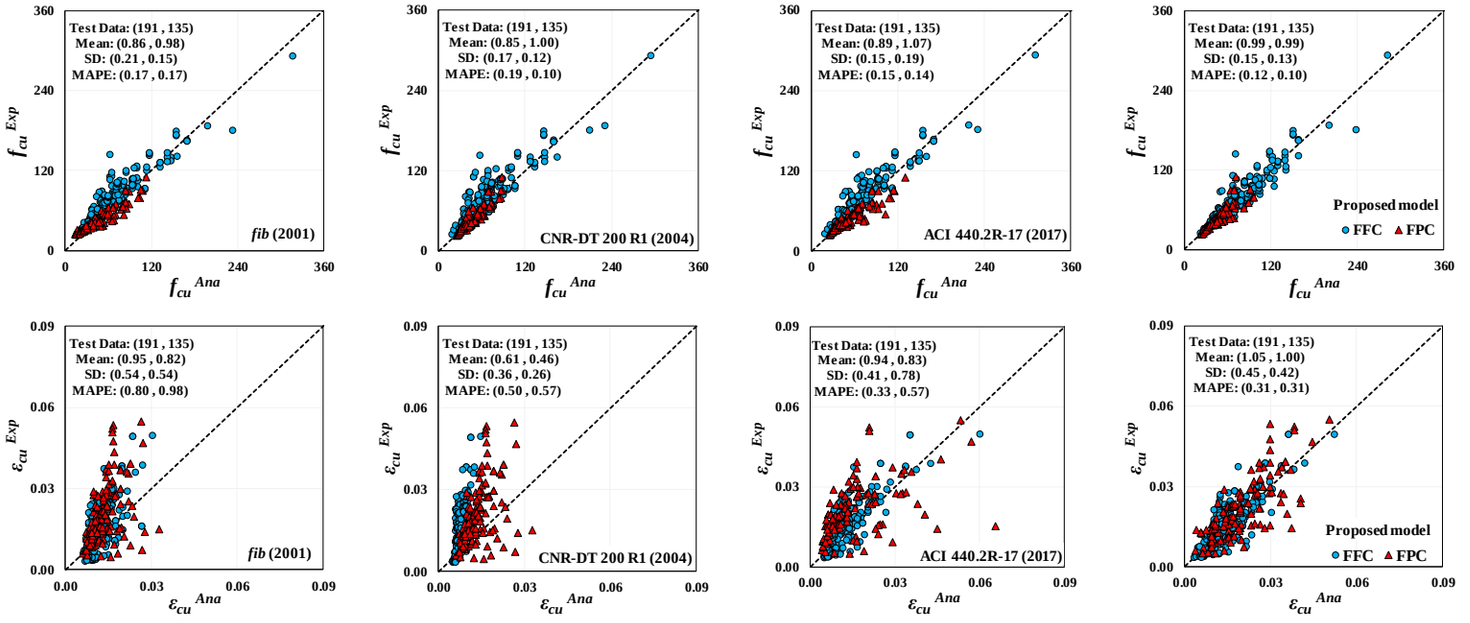

Fig. 16. Comparison of experimental results and analytical models

Fig. B.1

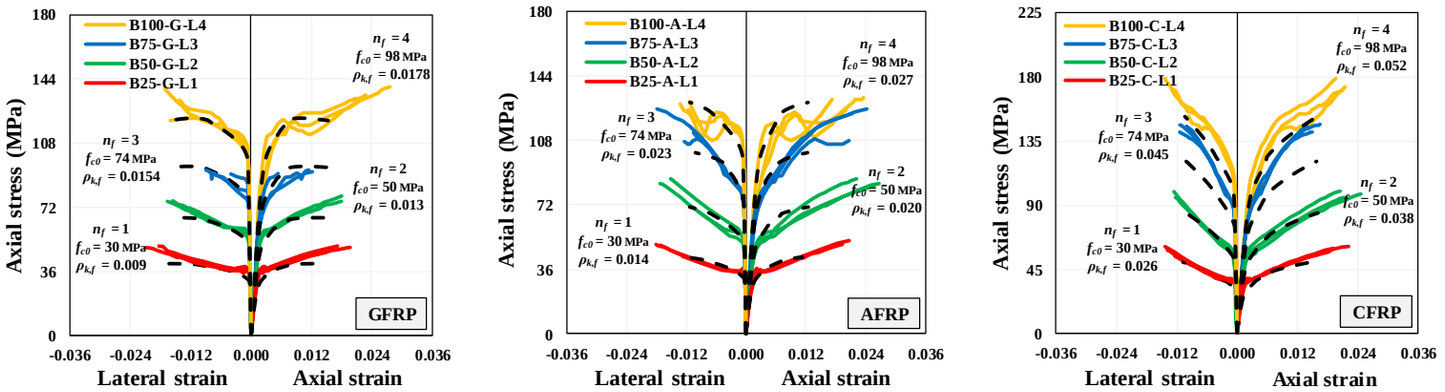

Fig. B.1. Analytical analyses versus experimental results for FFC specimens tested by Lim and Ozbakkaloglu [4]

Fig. B.2

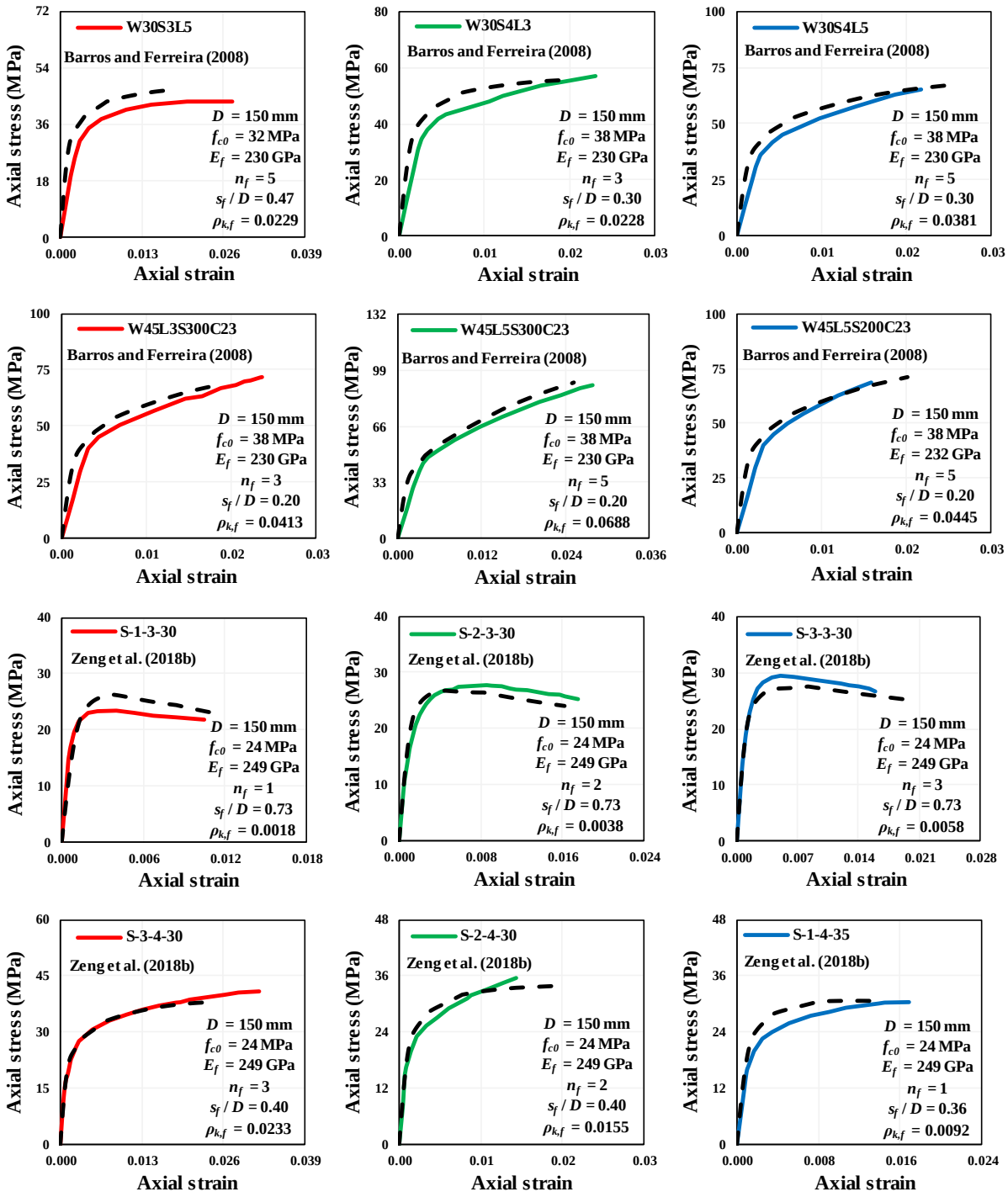

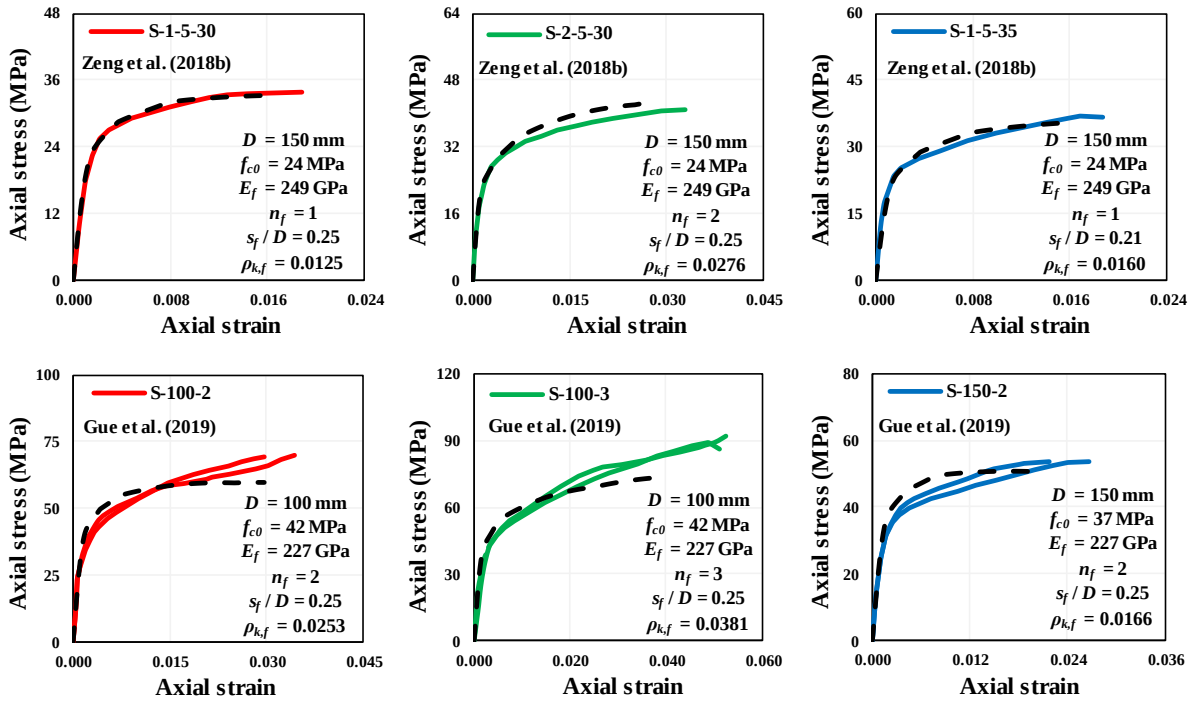

Fig. B.2. Analytical analysis versus experimental results for FPC specimens tested by Barros and Ferreira [6], Zeng *et al.* [7] and Gue *et al.* [8]

Table 1.

Table 1. Summary of confinement models for AFC and FFC

Model	Expression		Note
	Axial stress	**Peak axial stress**	
Category I	$f_c^{\ Active} = g_1\left(f_{cc}^{\ Active}\right)$	$\frac{f_{cc}^{\ Active}}{f_{c0}} = 1 + m_{a1}\left(\frac{f_l^{\ Active}}{f_{c0}}\right)^{m_{a2}}$	- $f_{cc}^{\ Active} = g_2\left(f_l^{\ Active}\right)$ - Confinement path-independent - m_{a1} and m_{a2} = calibration factors derived from AFC specimens
Category II	$f_c^{\ Passive} = g_1\left(f_{cc}^{\ Passive}\right)$	$\frac{f_{cc}^{\ Passive}}{f_{c0}} = 1 + m_{a1}\left(\frac{f_{l,f}^{*\ Passive}}{f_{c0}}\right)^{m_{a2}}$	- $f_{cc}^{\ Passive} = g_2\left(f_{l,f}^{*\ Passive}\right)$ - Confinement path-independent - m_{a1} and m_{a2} = calibration factors derived from AFC specimens
Category III	$f_c^{\ Passive} = g_1\left(f_{cc}^{\ Passive}\right)$	$\frac{f_{cc}^{\ Passive}}{f_{c0}} = 1 + m_{a1}\left(\frac{f_{l,f}^{*\ Passive} - \Delta f_l}{f_{c0}}\right)^{m_{a2}}$	- $f_{cc}^{\ Passive} = g_2\left(f_{l,f}^{*\ Passive}, \Delta f_l\right)$ - Confinement path-dependent - m_{a1} and m_{a2} = calibration factors derived from AFC specimens
		$\frac{f_{cc}^{\ Passive}}{f_{c0}} = 1 + m_{p1}\left(\frac{f_{l,f}^{*\ Passive}}{f_{c0}}\right)^{m_{p2}}$	- $f_{cc}^{\ Passive} = g_3\left(f_{l,f}^{*\ Passive}\right)$ - Confinement path-dependent - m_{p1} and m_{p2} = the calibration factors derived from FFC specimens

in which $f_c^{\ Active}$ is the axial stress of AFC as a function of peak axial stress ($f_{cc}^{\ Active}$); $f_c^{\ Passive}$ is the axial stress of FFC as a function of peak axial stress ($f_{cc}^{\ Passive}$) in the stress-strain base relation; f_{c0} is the axial compressive strength of unconfined concrete; Δf_l is the confinement pressure gradient; Confinement path represents the variation of confinement pressure with axial strain/stress.

Table 2

Table 2. Assembled database for FFC and FPC

ID	Total	Confinement arrangement		D (mm)	f_{c0} (MPa)	$\rho_{K,f}$	R_1	R_2	$\frac{f_{cu}}{f_{c0}}$	$\frac{\varepsilon_{cu}}{\varepsilon_{c0}}$
		FFC	FPC							
Rochette and Labossie`re [35]	**2**	2		100-150	44-45	2.6-4.2	1.97-2.35	0.75-0.86	1.6-1.7	7.2-7.7
Shehata *et al.* [36]	**2**	2		150	26-30	3.2-6.6	3.15-3.72	0.76-0.91	2.1-2.4	7.8-9.3
Teng and Lam [37]	**3**	3		152	37-39	1.5-3.9	3.15-3.82	0.64-0.80	1.4-1.9	4.5-8.2
Xiao and Wu [38]	**39**	39		152	34-55	1.3-8.5	0.62-3.81	0.68-1.05	1.0-2.8	1.9-12.7
Berthet *et al.* [39]	**15**	15		70-160	23.6-171	1.3-15.1	1.10-4.5	0.62-1.01	1.1.2.2	1.6-8.7
Barros and Ferreira [6]	**39**	8	31	150	18-40	0.1-26.2	0.18-4.86	0.34-1.40	1.0-6.5	2.9-28.1
Wang and Wu [30]	**4**	4		150	31-52	1.3-5.9	1.00-2.98	0.67-0.90	1.3-2.2	4.8-14.3
Eid *et al.* [31]	**18**	18		152	32-68	1.1-6.9	0.71-3.47	0.59-0.93	1.2-2.2	2.7-11.1
Wang and Wu [40]	**18**	18		70-194	24-52	0.3-5.1	0.19-2.85	0.37-0.89	1.0-3.4	1.5-6.0
Benzaid and Mesbah [41]	**6**	6		160	26-62	1.0-9.2	0.72-4.10	0.63-0.95	1.1-2.5	1.5-11.9
Lim and Ozbakkaloglu [4]	**36**	36		152	30-98	0.9-5.2	1.02-3.46	0.59-0.91	1.2-2.0	5.5-12.1
Vincent and Ozbakkaloglu [42]	**6**	6		152	110	2.7-4.8	1.16-1.73	0.80-0.90	1.2-1.5	5.4-6.9
Zeng *et al.* [43]	**12**	3	9	238	23	0.9-8.9	0.45-4.16	0.39-0.95	1.3-3.1	2.7-10.9
Zeng *et al.* [5]	**60**	6	54	150	23	0.1-13.0	0.20-4.25	0.31-1.16	1.1-4.7	5.2-26.8
Zeng *et al.* [7]	**15**		15	150	24	0.1-4.1	0.19-2.07	0.33-0.81	1.0-1.8	4.1-17.3
Wang *et al.* [44]	**7**	1	6	100	36	0.1-5.7	0.17-4.35	0.35-0.88	1.2-4.0	1.5-18.6
Guo *et al.* [8]	**21**		21	100-300	34-42	0.2-3.8	0.28-2.61	0.47-0.68	1.1-2.2	6.3-25.0
Suon *et al.* [45]	**3**	3		150	16	0.9-3.8	1.10-3.25	0.55-0.77	1.5-2.4	6.4-12.8
Shan *et al.* [46]	**3**	3		300	37	3.8	3.42	0.79	2.1-2.2	6.5-6.6
Lin *et al.* [17]	**18**	18		150	32-54	3.2-14.5	3.11-4.31	0.75-1.23	1.3-3.7	5.4-19.1
ALL	**327**	**191**	**136**	**155[a]-0.22[b]**	**40-0.56**	**3.6-0.94**	**1.79-0.65**	**0.68-0.37**	**1.8-0.38**	**9.3-5.9**

Note: a: Mean; b: CoV

Declaration of interests

☒ The authors declare that they have no known competing financial interests or personal relationships that could have appeared to influence the work reported in this paper.

☐The authors declare the following financial interests/personal relationships which may be considered as potential competing interests:

CRediT author statement

Javad Shayanfar: Conceptualization, Methodology, Data curation, Validation, Writing- Original draft preparation; **Joaquim A. O. Barros:** Conceptualization, Methodology, Writing- Reviewing and Editing, Supervision; **Mohammadali Rezazadeh:** Conceptualization, Methodology, Data curation, Writing- Reviewing and Editing.